Scholars' Mine

Summer 2017

Comparison of ²⁵²Cf time correlated induced fission with AmLi induced fission on fresh MTR research reactor fuel

Jay Prakash Joshi

Follow this and additional works at: https://scholarsmine.mst.edu/masters_theses

Part of the Nuclear Engineering Commons

Department:

Recommended Citation

COMPARISON OF ^{252}Cf TIME CORRELATED INDUCED FISSION WITH AmLi

INDUCED FISSION ON FRESH MTR RESEARCH REACTOR FUEL

BY

JAY PRAKASH JOSHI

A THESIS

Presented to the Faculty of the Graduate School of the

MISSOURI UNIVERSITY OF SCIENCE AND TECHNOLOGY

In Partial Fulfillment of the Requirements for the Degree

MASTER OF SCIENCE IN NUCLEAR ENGINEERING

2017

Approved by

Dr. Shoaib Usman, Advisor

Dr. Alexis C. Trahan, LANL Mentor

Dr. Ayodeji Babatunde Alajo

ABSTRACT

The effective application of international safeguards to research reactors requires verification of spent fuel as well as fresh fuel. To accomplish this goal various nondestructive and destructive assay techniques have been developed in the US and around the world. The Advanced Experimental Fuel Counter (AEFC) is a nondestructive assay (NDA) system developed at Los Alamos National Laboratory (LANL) combining both neutron and gamma measurement capabilities. Since spent fuel assemblies are stored in water, the system was designed to be watertight to facilitate underwater measurements by inspectors. The AEFC is comprised of six ^{3}He detectors as well as a shielded and collimated ion chamber. The ^{3}He detectors are used for active and passive neutron coincidence counting while the ion chamber is used for gross gamma counting. In the past, most of the active interrogation systems along with the AEFC were calibrated by AmLi neutron source. In this study, experiments were performed to calibrate the AEFC instrument and compare use of the ^{252}Cf spontaneous fission source and the AmLi (α,n) neutron emission source. MCNP simulations were carried out to benchmark experiments. This thesis analyzes time correlated induced fission (TCIF) from fresh MTR fuel assemblies due to ^{252}Cf and AmLi active interrogation sources. Benchmarking showed MCNP singles and doubles count rates agree with experimental singles and doubles within 5% and 4% respectively in the case of full assembly. After normalizing ^{252}Cf to the AmLi source strength, AmLi resulted 1.228 times more IF singles rate, while ^{252}Cf resulted 1.176 times more IF doubles rate. This indicates the boost in the doubles rate with ^{252}Cf source is due to the TCIF effect.

ACKNOWLEDGEMENTS

TABLE OF CONTENTS

LIST OF FIGURES

LIST OF TABLES

NOMENCLATURE

Acronyms	Description
AEFC	Advanced Experimental Fuel Counter
MTR	Material Testing Reactor
^{252}Cf	Californium-252 source
AmLi	Americium-Lithium source
SF	Spontaneous Fission
IF	Induced Fission
IAEA	International Atomic Energy Agency
NPT	Non-Proliferation Treaty
LANL	Los Alamos National Laboratory
HV	High Voltage
NPT	Nuclear Nonproliferation Treaty
NDA	Non-Destructive Assay
DA	Destructive Assay
^{235}U	Uranium-235 fuel
^{239}Pu	Plutonium-239 fuel
TCIF	Time Correlated Induced Fission
^{3}He	Helium-3 detectors
R	Real gate/count rate

A	Accidental gate/count rate
(α,n)	Alpha-neutron reaction
HDPE	High Density Polyethylene
HEU	Highly Enriched Uranium
LEU	Low Enriched Uranium
ADC	Analog to Digital Converter
DPRK	Democratic People's Republic of Korea
FA	Full Assembly (L-108)
PA	Partial Assembly (O-187R)
S	Singles Rate
D	Doubles Rate
MCNP	Monte Carlo N-Particle

Greek

σ	Uncertainty
ε	Neutron detection Efficiency
α	(α,n) to SF neutron ratio

1. INTRODUCTION

1.1. BACKGROUND

The Advanced Experimental Fuel Counter (AEFC) was originally designed to verify research reactor spent fuel. Initially, verification was focused on obtaining ^{235}U residual mass, burnup, and plutonium content. Plutonium was a part of the verification because it is produced in the fuel as it is being burned and could be used to make a weapon. The reason why residual ^{235}U mass is key is because during the first few decades in the early days of the research reactors, the fuel used was mostly highly enriched uranium (HEU) with approximately 90%, 80%, 60%, or 36% ^{235}U enrichment. [20] From the safeguards point of view ^{235}U can be separated from the HEU and can be used directly to make weapon. In the recent decades, efforts are being made to replace HEU fuel with LEU fuel. Uranium fuel is called LEU when ^{235}U enrichment in it is less than 20% by weight. [21] With LEU fuel, plutonium content becomes important from the safeguard's perspective as plutonium content increase vastly in the spent fuel as the fuel is changed from HEU to LEU due to the increase of ^{238}U content. If a country does not possess a reprocessing facility then plutonium content in spent fuel does not become critical, but in countries with reprocessing facilities, spent fuel verification becomes very important. Investigation of MTR fuel is crucial from the safeguards point of view as MTRs were installed in the countries that were committed to non-proliferation and their commitment needed verification.

This research focuses on the underwater verification of fresh MTR fuel using ^{252}Cf and AmLi active interrogation sources. ^{252}Cf source is used as an active source because of the difficulties in obtaining an AmLi source. It was found in the previous AEFC field trail that measurements with ^{252}Cf active sources resulted in doubles rates with lower uncertainty compared to when AmLi was used. It was seen that the time correlated neutrons in the background from ^{252}Cf did not hurt in the coincidence counting; rather, they reduced uncertainties.

The novel aspect of this research work is the underwater interrogation of highly enriched fresh MTR fuel assemblies with ^{235}U enrichment of 93%. The AEFC is the neutron coincidence system with underwater capabilities, which is shielded from the

fission product gamma rays when measuring spent fuel. The work focuses on the calibration of the AEFC with ^{252}Cf active source and fresh MTR fuel.

1.2.   HISTORY OF NUCLEAR PROLIFERATION

In 1939, Albert Einstein wrote a letter to the then President of the US, President Franklin D. Roosevelt, in which he showed his concerns that Germany might be close to having a fission based nuclear bomb, and stated how important it was for the USA to start its own program as soon as possible. [1] This urgency ultimately led to the production of first successful fission bomb in 1945, which was tested in the north of Alamogordo, New Mexico, USA, now known as a Trinity Site. Later, two bombs were dropped in the Japanese cities Hiroshima and Nagasaki. [2] The whole world witnessed the devastation that nuclear weapons did to the two Japanese cities. The World War II ended, however the fear of the nuclear weapon rose. Over the past 71 years many countries aspired to produce their own nuclear weapon, some were successful while others were not. Almost all those countries justified their aspiration with the need for national security and to enhance their international status. [3]

By 1952, three countries, USA, UK, and Russia, had already produced nuclear weapons. The world was already beginning to witness a proliferation of nuclear weapons. The US President Dwight D Eisenhower gave a speech in New York to the UN General assembly on "Atom for Peace" in 1953 as he understood the danger of excessive unmonitored nuclear material. In his speech he proposed formation of the IAEA, which got an international focus. The creation of IAEA created nuclear safeguards as well as expanded peaceful use of atoms. [4]

The NPT was drafted in 1965 in the Geneva disarmament conference, which banned further acquisition and transfer of nuclear weapons. This was direct effect of the US President John F. Kennedy, as he described the "Greatest global threat of the future to be as many as 25 states owning nuclear weapons." The treaty entered into effect in 1970 with 43 member countries including the Soviet Union, the US, and the UK. The missions of the NPT were non-proliferation, peaceful use of atom, and disarmament. The treaty clearly stated that it would help states build a research and commercial power plant capabilities for the peaceful use. [4]

DPRK ratified the NPT in 1985, which is almost two decades after they received their first research reactor from the Soviet. North Korea continued its nuclear weapons program while they were NPT member state. The North Korea incident clearly indicated the flaws in the treaty. It showed if a country signs NPT, IAEA would help train and build nuclear technology and infrastructure for that country, but IAEA did not have sufficient authority to investigate undeclared facilities and at the same time a country could withdraw from NPT any time. NPT was not effective in implementing non-proliferation mission of IAEA. There was a need of additional protocol, a strong infrastructure for the timely detection of diversion of any significant quantities of special nuclear material from peaceful nuclear activities to the manufacture of nuclear weapons, and the ability to verify the operator's declared fuel parameters such as initial enrichment, burnup, cooling time, and the fissile mass content of the spent fuel. [4]

With an increase in the number of nuclear facilities around the world, faster, efficient, effective, and accurate ways to investigate spent as well as fresh fuel is becoming increasingly important. Nondestructive assay (NDA) techniques have been very useful for the IAEA safeguards for treaty monitoring and verifying nuclear activities. The most important work of IAEA safeguard is to make sure nuclear material is not diverted for weapons purpose. The AEFC is one of the nondestructive assay (NDA) systems designed to account and verify nuclear material in a research reactor and make sure that nuclear material is not diverted for weapons purposes.

1.3.   NDA TECHNIQUE

NDA is an important tool for nuclear material safeguards to verify the nuclear material inventory. The NDA technology was started more than 50 years ago in mid 1960s during the time when the NPT was written. [9] Over the past 50 years, there have been significant improvements in NDA techniques and instrumentation. Many of the improvements are in detection capabilities such as highly efficient detectors, and electronic processing such as better preamplifiers, amplifiers, analog to digital converters, and data analysis. There have been developments of better computer software for the analysis of the data generated in the measurements. Better computing power has helped in the advancement of NDA techniques by allowing large data collection and complex Monte Carlo simulations and calculations.

NDA can be used in all steps of nuclear fuel cycles such as mining/milling, fabrication plant, enrichment plant, reactor operation as well as in the backend of fuel cycle. The technique is used to identify any undeclared material and operation, and verify operator declared fuel parameters such as initial enrichment, burnup, cooling time, residual fissile mass, or any diverted assembly from a reactor core or a spent fuel pool. The NDA systems can collect and store data from different detectors simultaneously, and at the same time analyze data immediately after the measurement completion. [9]

Unlike destructive analysis (DA), in which the fuel sample is physically destroyed for the sample fuel characterization, the AEFC is one of the NDA techniques that use neutrons and gamma ray signals from the fuel sample. DA techniques are more accurate than NDA because they use techniques like mass spectroscopy in which material is characterized relative to reference standards.

Spent fuel is heterogeneously irradiated, which results in there being more burnup at the middle of the fuel assembly compared to the ends in axial direction. This scenario makes DA techniques difficult and time consuming because there would be a need to account for the errors in sampling. In DA techniques, the whole sample is broken and grinded to make a homogenous sample, whereas in fact the fuel is heterogeneously burned in a reactor. The change in neutron and gamma signals are discrete axially, therefore fuel would have to be broken into many pieces axially and grinded separately to get accurate results in the DA. This whole process is complex and comes with contamination risks as fuel sample should be physically broken. NDA techniques such as the AEFC are faster, easier, less hazardous, and can be repeated as many times as required. The IAEA inspectors have been using NDA techniques to verify and characterize spent fuel for decades due to these attractive options offered by the NDA techniques. [2]

1.4.   ADVANCED EXPERIMENTAL FUEL COUNTER (AEFC)

The AEFC is a NDA system developed at the LANL combining both neutron and gamma measurement capabilities. Since spent fuel assemblies are stored in water, the system was designed to be watertight to facilitate underwater measurements by inspectors. The AEFC is comprised of six ^{3}He detectors as well as a shielded and collimated ion chamber. The ^{3}He detectors are used for active and passive neutron

coincidence counting while the ion chamber is used for gross gamma counting. Active coincidence measurement data is used to measure residual fissile mass (i.e., ^{235}U + ^{239}Pu), whereas the passive coincidence measurement data along with passive gamma measurement can provide information about burnup, cooling time, and initial enrichment. [5]

The SF source ^{252}Cf was successfully used as an active interrogation source in lieu of AmLi in the 2014 field trail in Uzbekistan by Menlove et al. [5]. Before that, ^{252}Cf was thought to be unfavorable as an active interrogation source because it would produce a background of time correlated neutrons during each fission event. While AmLi produces random neutrons in time with no active source background coincidences, ^{252}Cf gives a complex coincidence background. [6]

Table 1-1 shows active and passive signals that can be acquired from the spent fuel measurements using the AEFC detection system. The table shows that in passive mode total singles rate is the sum of SF and (α,n) reaction, while the total doubles rate come from just SF. Ionization chamber provides the information about the relative burnup and a burnup profile by measuring gross gamma counts after cooling time corrections. In the active interrogation mode, total singles and total doubles rates come mostly from IF events.

Table 1-1: AEFC Operating Parameters and Signals [5]

Measurements	Fuel Attribute
Passive Interrogation Signals	
Singles rate (^{3}He detector)	SF + (α,n)
Doubles rate (^{3}He detector)	SF
Ion chamber	Relative Burnup (^{137}Cs) + profile
Active Interrogation Signals	
Singles rate	IF
Doubles rate	IF

2.   THEORY AND BACKGROUND

2.1.   NEUTRON DETECTION MECHANISM

Neutrons are neutral, and do not interact with electrons in an atom unlike gamma rays or alpha particles. Neutrons interact with the nucleus, which results in a release of one or more charged particles. The charged particles are then detected and processed by the detection systems. Scattering and nuclear reactions are two basic neutron interactions. Scattering interaction is effective only with the light nucleus such as hydrogen and helium, in which neutron transfers enough energy to create a recoil nucleus. Recoil nucleus ionizes surrounding material inside the detector. The ionization results in a release of particles such gamma rays, alpha, beta, or x-rays that are ultimately detected. In the case of nuclear reaction, the products such as gamma rays, proton, alpha, or the fission fragments are detected. In both cases, the electrical signal produced by the charged particles or gamma rays are detected. Both the cases are indirect measurement of neutrons. [8][16]

2.2. ^{3}He PROPORTIONAL NEUTRON DETECTORS

When a neutron reacts with ^{3}He nuclides, energetic charged particles are released into gas inside the detector. The charged particles ionize surrounding gas molecules, which causes avalanche process that leads to detection. The energy released from a nuclear reaction is deposited in the detector. When ^{3}He reacts with the neutron, the reaction gives off a tritium, a proton, with 765 KeV energy shared between two nuclides. The reaction that occur inside the detectors containing ^{3}He is given in Equation 1 below: [7][8][16]

$$^3\text{He} + \text{n} \rightarrow {}^3\text{H} + {}^1\text{H} + 765 \text{ KeV} \tag{1}$$

^{3}He detectors are used widely in verifying and accounting nuclear material by the IAEA inspectors. The detectors are used to perform coincidence counting to verify a fissile mass in a fresh and spent fuel as well as monitor fuels in all phases in a nuclear fuel cycle. To possess capabilities to discriminate pulses created by the gamma interactions, ^{3}He detectors are operated in proportional region rather than operating in Geiger region. The neutron absorption cross section of ^{3}He follows $1/v$ relationship in a

thermal region up to approximately 200 KeV, where v is a neutron velocity. ^{3}He is very sensitive to the thermal neutrons as it has a high thermal neutron cross section of 5330 barns. [8] Since ^{3}He has high thermal neutron cross section, the detectors are put inside the neutron moderator such as water or high density polyethylene during entire measurements process. [7][8][16]

^{3}He detectors use ^{3}He(n,p)^{3}H nuclear reaction to detect moderated neutrons. Released charged particles, a proton (^{1}H$_1$) and a triton (^{3}H$_1$) produce electrons that are attracted by the anode wire's high voltage. The electrons accelerate towards anode and create a detection cloud via charge multiplication. A charge sensitive amplifier detects a charge induced by a detection cloud nearby to the cathodes by means of capacitive coupling. Figure 2-1 below shows visual representation of a pulse height spectrum of typical ^{3}He detector. [7][8][16]
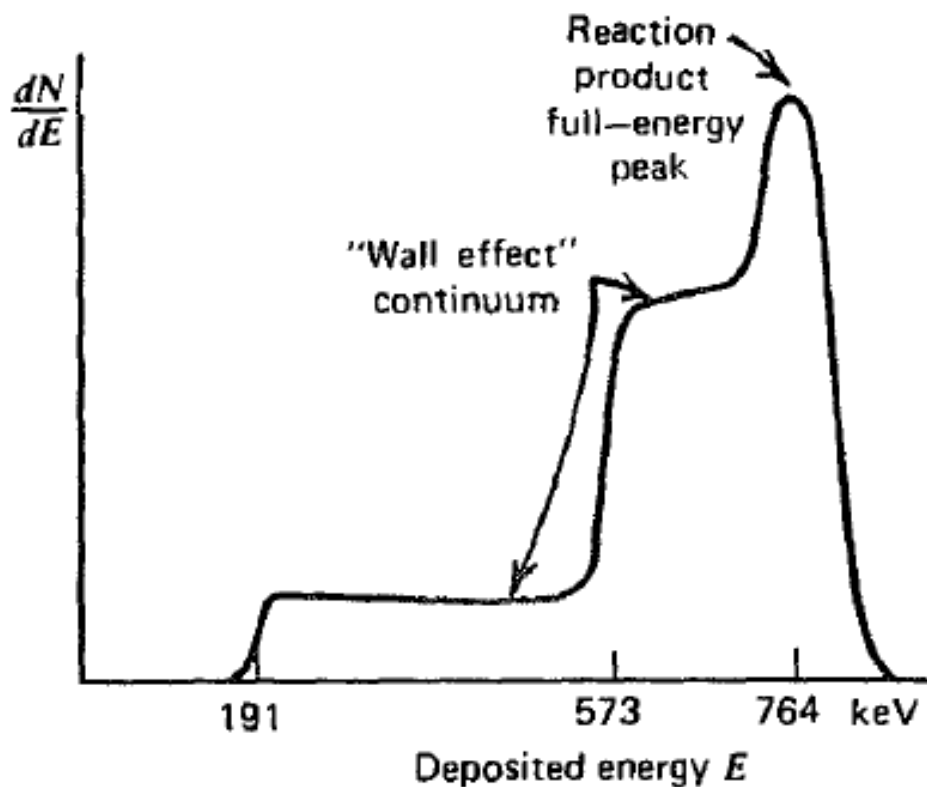
Figure 2-1: Pulse height spectrum from ^{3}He detector [8]

The Q-value of the nuclear reaction is approximately 765 KeV and the energy is carried by the daughter products in the form of kinetic energy. Since the emission of daughter products follow conservation of momentum, the daughter products travel in opposite direction. Possibility of energy deposition depends on only one daughter register, both daughters escape, or both daughter register kinetic energy in the detector, however the output pulse is proportional to 765 KeV. [7][8][16]

The main peak at 765 KeV in Figure 2-1 is a kinetic energy liberated in a ^{3}He and thermal neutron nuclear reaction. By the law of conservation of momentum, less energy is carried by heavier ^{3}H daughter compared to the lighter ^{1}H. Approximately 191 KeV and 574 KeV of kinetic energy are split between ^{3}H and ^{1}H daughter nuclides respectively. If a reaction occurs close to the detector wall, one of the two daughter nuclides might get absorbed in the wall while trying to escape from the detector and other might get absorbed in the detector gas. Because of this wall effect peaks at 191 KeV and 573 Kev along with long plateau is seen in a pulse height spectrum of ^{3}He detector. [7][8][16]

2.3.   ROSSI-ALPHA DISTRIBUTIONS

To explain coincidence counting, the Rossi-Alpha distribution should be well understood. Rossi-Alpha distribution is a probability distribution of the time interval between neutron pulses detected during the measurement process. Figure 2-2 demonstrates the Rossi-alpha distribution, where P is a pre-delay, G is a gate length, and D is a long delay gate.

Neutrons produced in induced fission event in the same fission chain in a fuel assembly are time correlated. The purpose of R-A distribution in the AEFC is to experimentally determine a probability distribution of detecting time correlated neutrons released from the same fission event. First neutron detected inside any of six ^{3}He detectors acts as a trigger and opens a time window. All neutrons detected within that specified time window are time correlated coincidences to the initial triggering neutron. Subsequently, each neutron after the first triggering, neutron triggers its own window of equal time length and thus a distribution is produced. If a random source (AmLi) is measured, a flat distribution will be obtained, but if a source that emits time correlated

neutron (^{252}Cf) is measured, the distribution obtained will look like an exponential function. The distribution in Figure 2-2 is described by the Equation 2 below.

$$S(t) = A + Re^{-t/\tau} \tag{2}$$

Where A is accidental coincidence, R is real coincidence, and τ is the die away time. [6][9]
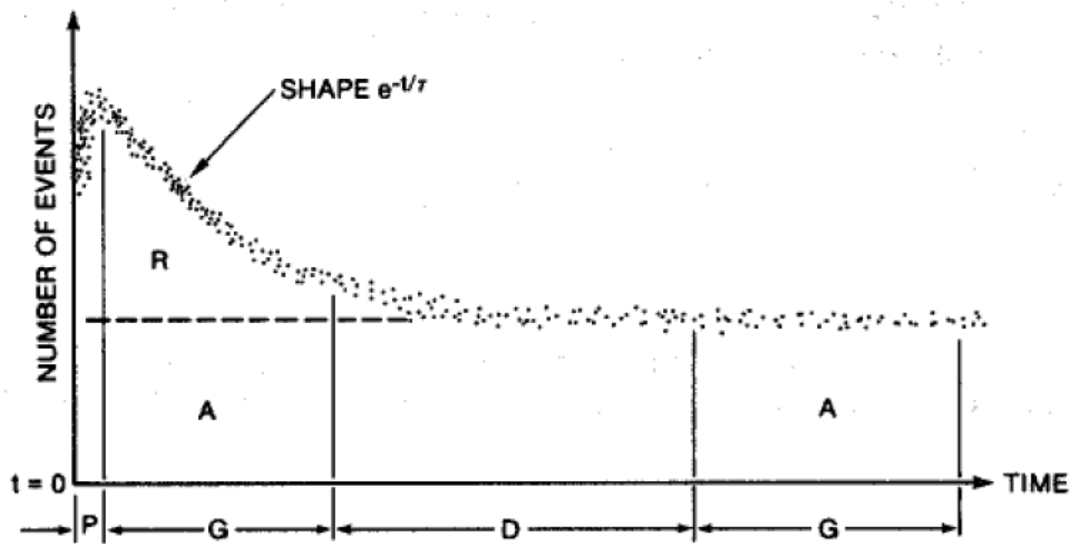
Figure 2-2: Rossi-Alpha distribution [9]

The accidental rate is proportional to the square of totals rate and is given by the Equation 3. [10]

$$A = GT^2 \tag{3}$$

In Equation 3, G is a gate length and T is a totals rate. The totals rate consists of both accidental rates as well as real rates. [10]

Figure 2-3 represents a train of electronic pulses. The pulse train (a) represents an ideal pulse train that contains easily distinguishable correlated and uncorrelated pulse train events, however pulse train (b) is the real pulse trail that is obtained during the measurements. The case (b) is complex as correlated and uncorrelated events cannot be separated easily.
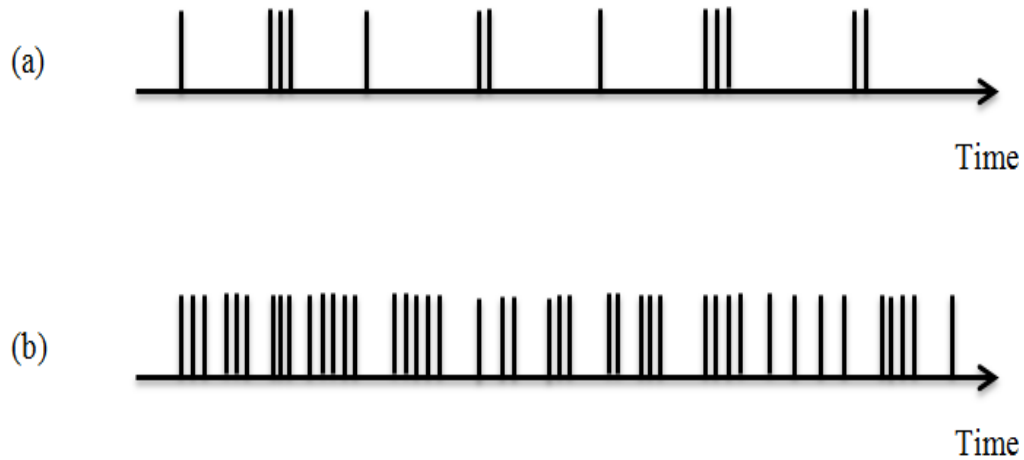
Figure 2-3: Neutron pulse train in a time axis [6][9]

Table 2-1 below provides the specifications of ^{3}He detectors and preamplifiers and their operating parameters such as pressure inside the detector tubes, operating voltage range, gate length, pre-delay, and detector die away time used in the AEFC system.

Table 2-1: Detectors and Amplifier Specifications [5]

Parameter	Values
Number of detector tubes (RS-P4-0810-119)	6
Diameter of ^{3}He detector	25.4 mm
Active length of ^{3}He detector	254 mm
Pressure inside the detector tube	4 Atmosphere
Operating Voltage	1640-1680 V
PDP-10A preamplifiers	6
Die-away time	85 μsec
Gate	128 μsec
Pre-delay	4.5 μsec

2.4.   NEUTRON COINCIDENCE COUNTING

The AEFC consists of six ^{3}He detectors that use coincidence counting to characterize research reactor fuel. For example, a SF event in ^{252}Cf releases in average 3.76 neutrons, and these neutrons then cause IF in a fuel assembly. On average 2.44 neutrons are released from ^{235}U IF event. If only one out of an average 3.76 neutrons from ^{252}Cf source is captured inside a fuel assembly and causes IF, an average of approximately 5.2 neutrons will be released in the whole process that are time correlated. Although coincidence detection depends on the efficiency of detection system, there is an increase in effective average neutrons per fission (v). [6][11]

If two neutrons are detected by any of the six ^{3}He detectors within the specified time window 128µsec, they are defined as coincidences. There is a chance that the coincidences measured are accidentals from background and active source, but these accidentals can be separated from the real coincidences from fuel. The process of separation is explained by the Rossi-Alpha distribution, which is explained in Section 2.3 below. The probability of detecting uncorrelated neutrons increases with the increase in active interrogation source strength; however, these uncorrelated neutrons can be separated statistically. [6][9]

Shift register is used to acquire neutron coincidence data in a measurement. Shift register opens a pre-delay and gate for each neutron detected in any of six ^{3}He detectors, and gives a recovery time to the detectors to perform coincidence counting. The shift register opens a pre-delay of 4.5 µs each time a trigger occurs in order to eliminate the dead time effect. After a pre-delay, it opens R+A and A gates of 128 µs separated by a long delay. A long delay is several die away times of a neutron that triggers a pre-delay. Due to the long delay (~ 1000µs), coincident neutrons detected in accidental gate (A) are true accidentals because after the long delay all neutrons from the precursor triggering Sf or IF events are already gone. The neutrons counted after a long delay are just accidentals and they are constant throughout the A gate. The visual representation of R+A and A gates can be seen in Figure 2-2 in Section 2.3. The real coincidence is then given by the Equation 4 below: [6][9]

$$R= (R+A) - A \qquad\qquad (4)$$

The coincidence counting statistics is complex due to the presence of real and accidental pulse trains. The shift register has to discriminate between the real and accidental count rates as well as provide uncertainties of measurements related to these count rates. In general, in a shift register uncertainty in real count rate is given by the Equation 5. [10]

$$\frac{\sigma_R}{R} = \frac{\sqrt{((R+A)+A)}}{R} = \frac{\sqrt{(R+2A)}}{R} \tag{5}$$

In the case of JSR-15 shift register used in this research, accidental gate A triggers on clock frequency of approximately 50MHz therefore accidentals rates are counted a lot more than the R+A gate. This makes contribution of A rates in the measurement uncertainty negligible. Then the uncertainty in R measurements depends only on R+A uncertainties. The JSR-15 shift register uncertainty in real count rate is given by the Equation 6. [10]

$$\frac{\sigma_R}{R} = \frac{\sqrt{(R+A)}}{R} \tag{6}$$

The measurement uncertainty for random neutrons is different process than when the correlated neutrons. Random neutrons follow Poisson distribution therefore when the number of counts is n neutrons the relative error is given by the Equation 7. [10]

$$\frac{\sigma_n}{n} = \frac{Var(n)}{n} = \frac{1}{\sqrt{n}} \tag{7}$$

While correlated neutrons such as from SF do not follow Poisson distribution, the numbers of SF events follow Poisson distribution. If a total number of neutrons emitted in SF is T, $\bar{v}$ is an average SF multiplicity, and the number of SF events is S, then, [10]

$$T = \bar{v}S \tag{8}$$

The relative error for measuring n correlated SF neutrons with the absolute detector efficiency ε this given by,

$$\frac{Var(n)}{n} = 1 + \varepsilon \frac{\overline{v^2} - \bar{v}}{\bar{v}} \tag{9}$$

In the Equation 9, the variance approaches Poisson distribution when $\bar{v}$ approaches 1 or ε approaches 0. Therefore, the measurement uncertainty of SF in coincidence counting depends on multiplicity and absolute detector efficiency. [10]

2.5.   DIE-AWAY TIME

When neutrons are emitted from a source, two events are possible, (1) they can travel for ever until they decay or (2) interact with matter until it gets absorbed. Neutrons may scatter multiple times and ultimately get absorbed or decay away. All neutron detection systems have a neutron die away time, which is an average neutron lifetime in a detector system after which neutron emitted from a fission event either decayed away or are captured in some material in the system. Neutrons are removed from a system by getting captured in a detector tube, absorption in a surrounding material, or leakage from a system. The die away time in a system is represented by an exponential decay of the form: [9]

$$N(t) = N(0)e^{-t/\tau} \tag{10}$$

In Equation 10, N(t) is a neutron population at time t and τ is a die away time, a mean lifetime in the system. Different systems have different size, shape, material composition, and efficiency. The AEFC system has a gate width of 128μsec, which is greater than the die away time of the AEFC system. Typically, most systems have die-away time ranging 30 to 100 μsec. [9]

The die away time of a detection system can be determined by experimental measurements. It is done by measuring the same sample with the same settings and procedures except two different gate G_1 and G_2 where G_1 is half of G_2. Two coincidence rates R_1 and R_2 will be obtained corresponding to gate G_1 and G_2. The die away time is given by the Equation 11 below. [6]

$$\tau = -\frac{G_1}{\ln(R_2/R_1 - 1)} \tag{11}$$

2.6.   NEUTRON MULTIPLICITY AND MULTIPLICITY COUNTING

Multiple neutrons and gamma rays are emitted in each fission reaction. Neutrons that are emitted within 4×10^{-14} seconds are prompt neutrons, while delayed neutrons are

emitted roughly within tenth of a second of scission and the delayed neutron population is very small compared to the prompt neutron population. Neutron Multiplicity (ν) is defined as the average emission of neutrons during the fission event of some nuclide. Average number of neutrons emitted per fission event varies depending upon the isotope and it is distributed from 0 to 8 or more neutrons per fission. This neutron distribution is a multiplicity distribution that contains the sum of 0, 1, 2, 3, 4, 5, 6, 7, 8, or more neutrons within the coincidence gate width. An example of multiplicity distribution of ^{252}Cf is shown in the Figure 2-4 below. [13]
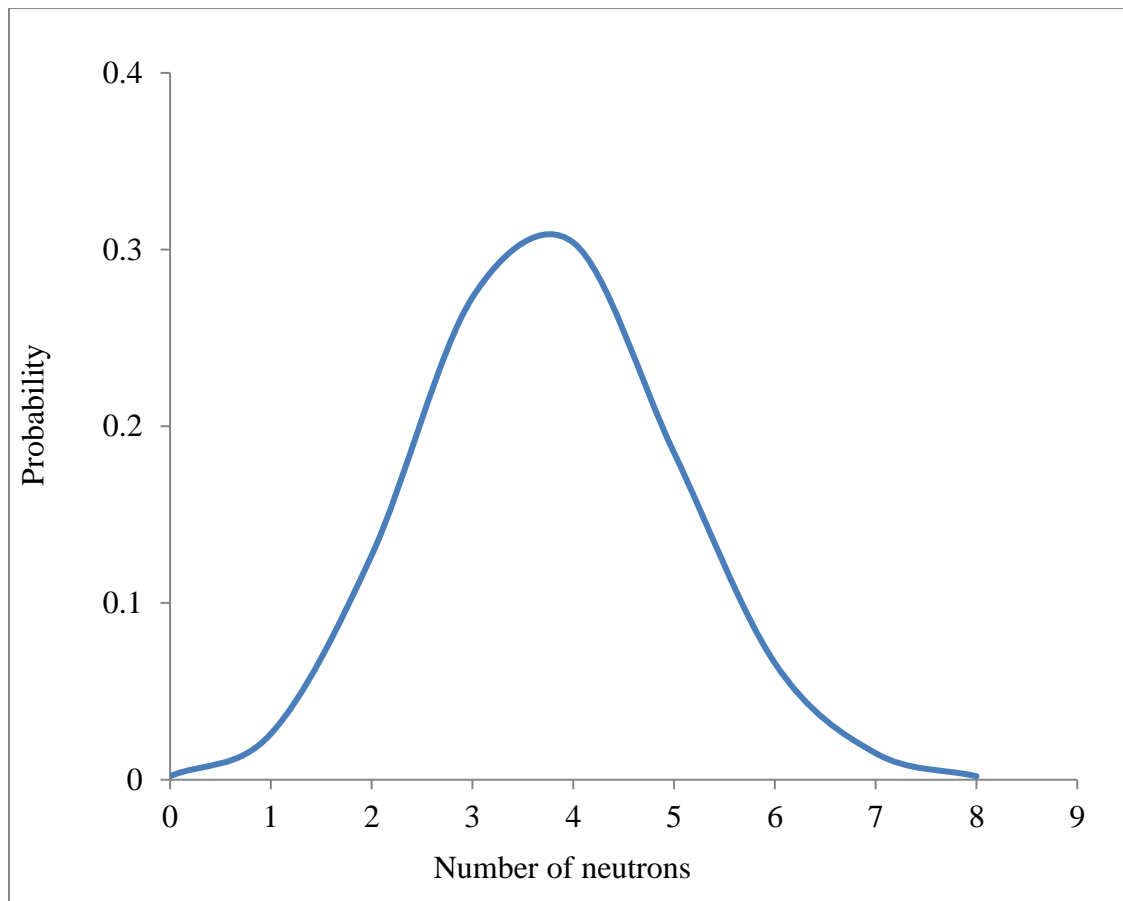
Figure 2-4: Measured prompt fission multiplicity distribution of ^{252}Cf [15]

Multiplicity is based on the factorial moments, where first moment yields singles, second moment yields doubles, and third moment yields triples, and so on. While

coincidence counting deals with singles and doubles, multiplicity counting allows analyzing higher order moments such as triples, quads, etc. Multiplicity counting is just an extension of coincidence counting to the collection of higher multiples of neutrons. Singles, doubles, and triples follow the following three Equations 12, 13, and 14 given below. [6][9][11][22]

$$\text{Singles} = F\varepsilon M v_{s1}(1 + \alpha) \tag{12}$$

$$\text{Doubles} = \frac{F\varepsilon^2 f_d M^2}{2}\left[v_{s2} + (M-1)\frac{v_{s1}v_{i2}}{v_{i1}-1}(1+\alpha)\right] \tag{13}$$

$$\text{Triples} = \frac{F\varepsilon^3 f_t M^3}{6}\left[v_{s3} + (M-1)\frac{3v_{s2}v_{i2}+v_{s1}v_{i3}(1+\alpha)}{v_{i1}-1} + 3\frac{(M-1)^2}{(vi_1-1)^2}v_{s1}(1+\alpha)v_{i2}{}^2\right] \tag{14}$$

where F is spontaneous fission rate, ε is neutron detection efficiency, M is neutron leakage multiplication, α is (α,n) to SF neutron ratio, f_d is doubles gate fraction, f_t is triples gate fraction, v_{s1}, v_{s2}, and v_{s3} are factorial moments of the spontaneous fission neutron distribution, and v_{i1}, v_{i2}, and v_{i3} are factorial moments of the induced fission neutron distribution. [22]

2.7. SELF SHIELDING

The material composition of MTR fuel is uranium Aluminum Alloy. The uranium atoms in UAl are mostly ^{235}U and ^{238}U isotopes. ^{235}U and ^{238}U have high thermal neutron absorption cross section, which gives rise to the self-shielding inside the fuel assembly. The neutron flux in the fuel assembly gets reduced because of this self-shielding effect. When thermal neutrons pass through the fuel, some get absorbed inside the fuel and some scatter before the rest escape from the fuel. ^{235}U has a high fission cross section along with the high absorption cross section in thermal region, therefore when it absorbs neutron it will either transmute to another nuclide or fission and produce some more neutrons, but ^{238}U has a very small fission cross section, so when it absorbs neutrons they are typically lost.

The research reactor fuel assemblies might contain different ^{235}U enrichment ranging from 10% to 93%. For the fuels that are enriched 10%, self-shielding is mostly by ^{238}U while some by ^{235}U. For the fuels that are enriched 93%, the self-shielding is

mostly due to [235]U. Multiplication is significantly higher in a fuel with 93% enriched fuel compared to the 10% enriched because of the difference in [235]U mass. [6][12]

2.8.   [252]Cf SF SOURCE

SF occurs due to a quantum tunneling mechanism effect rather than by interacting with other neutrons like in IF. The nucleus gets to the scission point from its ground state by tunneling through the fission barrier. In this process, a heavy nucleus splits into two or more smaller fragments without any external impact, which is due to an opposition between the attractive nuclear forces and columbic repulsive force. Nuclear force holds nucleons in the nuclei, whereas coulomb repulsion drives the protons apart. In case of lighter nuclei, repulsive Coulomb force is easily overwhelmed by a nuclear force, however in case of heavier nuclei, repulsive Coulomb force dictates over nuclear force, hence SF is observed in heaver nuclei. [13]

In the AEFC, a SF source, [252]Cf, is used as an active interrogation source. [252]Cf is an actinide which emits an average of 2.34×10^{12} n/s per gram and decays with an effective half-life of 2.57 years. Since [238]U must undergo 14 transmutations to produce a [252]Cf isotope, very small amount is produced in a nuclear fuel. For example, about 0.025 grams of [252]Cf is produced by the Oak Ridge National lab every year from feedstock at Savannah River Site. Though the production is a small quantity, a very small amount of [252]Cf is enough to make a source. [17]

$$^{252}_{98}Cf \rightarrow ^{94}_{38}Sr + ^{154}_{60}Nd + 3.76n \qquad (15)$$
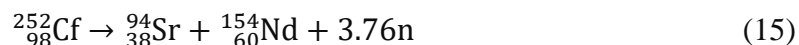
Average number of spontaneous neutrons from [252]Cf is 3.76 neutrons and the average energy of the fission neutron spectrum is 2.3 MeV. The advantages of [252]Cf sources such as intense neutron concentration, long half-life of 2.57 years, higher average neutron yield of 3.76 neutrons per fission, substantial neutron output of 2.34×10^{12} n/s, and its availability makes it a very good candidate for use as an active neutron source. [6][8]

2.9.   AmLi, (α,n) NEUTRONS SOURCE

The AmLi (α,n) random source is used as active interrogation source in the AEFC. [241]Am in AmLi is a transuranic element or actinide, which is produced during a transmutation of [238]U isotope in a nuclear fuel. Over the time there is a buildup of

Plutonium-241 in burned fuel. [241]Pu decays with a half-life of 14.4 years to produce [241]Am whose half-life is approximately 432.7 years. [241]Am then decays to neptunium-237 by emitting an alpha particle with an average energy of 5.46 MeV. [237]Np is stable as it decays very slowly with a half-life of 2 million years. [241]Am can be combined with lighter elements such as lithium (Li) or beryllium (Be) to produce neutrons. [14]

$$^{241}_{95}\text{Am} \rightarrow \, ^{237}_{93}\text{Np} + \, ^{4}_{2}\alpha + \gamma(59.54 \text{ KeV}) \tag{16}$$

$$^{4}_{2}\alpha + \, ^{7}_{3}\text{Li} \rightarrow \, ^{1}_{0}\text{n} + \, ^{10}_{5}\text{B} + Q(\text{value}) \tag{17}$$
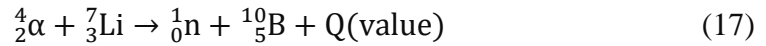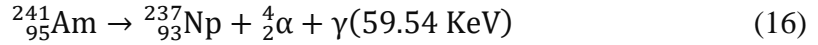
It is difficult to obtain AmLi in the US because it contains lithium which is highly flammable.

2.10. TCIF EFFECT IN THE AEFC WITH [252]Cf

TCIF term was brought up by Dr. Howard Menlove at the LANL. [17] The TCIF effect comes from the neutrons emitted in IF events in the fuel assembly coupled to the neutrons produced in a precursor fission event in an active interrogation source. When [252]Cf is used as an active interrogation source, the trigger event to start coincidence gate can be caused either due to the IF neutron from the fuel or SF neutron from the active source. The multiplicity (ν) in [252]Cf is 3.76 and multiplicity in IF is 2.44, therefore the combined multiplicity is much higher when [252]Cf is used compared to the combined multiplicity with AmLi (α,n) source. When the effective multiplicity increases, the coincidence rates such as doubles increase as well. [17]

Also, the TCIF measurements in the AEFC depend on the coupling probabilities between the active source, fuel assembly, and the six [3]He detectors. Coupling between active source and fuel sample resulting in IF (P_1), at least one neutron from IF is detected in any of the six [3]He detectors (P_2), and finally the active source background getting detected in any of the six [3]He detectors (P_3) are the three coupling probabilities that makes up the combined probability in the AEFC. P_1 is a function of effective fission cross section, distance between active source and the fuel, and HDPE moderator, P_2 depends on the detector efficiency to detect neutrons induced from the fuel, and P_3 depends on the detector efficiency to detect neutrons from the active source. These coupling probabilities P_1, P_2, and P_3 are very low in the AEFC. The combined probability determines the extent of coincidence rate boost due to the TCIF effect. Even though the coupling probabilities between the three regions are very low, on average, the

measurements result with ^{252}Cf is expected to show significant increase in the doubles rate compared the doubles rate when AmLi source is used. The neutrons produced from the fuel have the highest probability of detection than the neutrons emitted from active source, therefore when multiple correlated neutrons are produced via multiple correlated neutron induced fission events in the fuel, they're more likely to be detected resulting in a higher coincidence count rate. [17].

The experimental measurements show the efficiency of active source background for ^{252}Cf and AmLi to be 0.94% and 0.59% respectively. The reason behind the lower efficiency for AmLi active background is due to the over-moderation of lower energy AmLi neutrons causing fewer neutrons to reach the detectors. With the fuel assembly included in the AEFC, efficiency of net IF (defined as IF-active background) with AmLi changes to 1.19%, while it changes to 0.987% for ^{252}Cf. Higher efficiency for AmLi IF is due to the under-moderation for the neutrons to reach fuel assembly, meaning that the lower energy AmLi neutrons can reach thermal energies and induce fission more easily than those from ^{252}Cf. Even though AmLi produced 1.21 times more singles count rates from interrogation of the fuel than ^{252}Cf, ^{252}Cf interrogation of the fuel produced more doubles count rates. This proves that the boost in the doubles count rate is due to boost in combined multiplicity of IF+SF due to the TCIF effect. [6][11][17]

Figure 2-5 represents possible scenarios that could happen inside the AEFC system in presence of fuel assembly inside the fuel through hole and active source inside the source hole. In the Figure 2-5, part a shows SF neutrons both being detected and inducing fission in the fuel, causing a boost in coincidences due to the TCIF effect. Part b shows none of the 4 neutrons from SF getting absorbed in a fuel. In this case the doubles rate is due to the neutrons from SF. Part c shows all neutrons from SF event escape the system, hence no counts registered. Part d shows another coincidence boost due to the TCIF effect in ^{252}Cf. Part e shows an (α,n) neutron escaping the system resulting in no detections. Part f shows a neutron from AmLi undergoing multiple scattering events before being detected. Part g shows a neutron detected from an IF event caused by an AmLi source neutron.
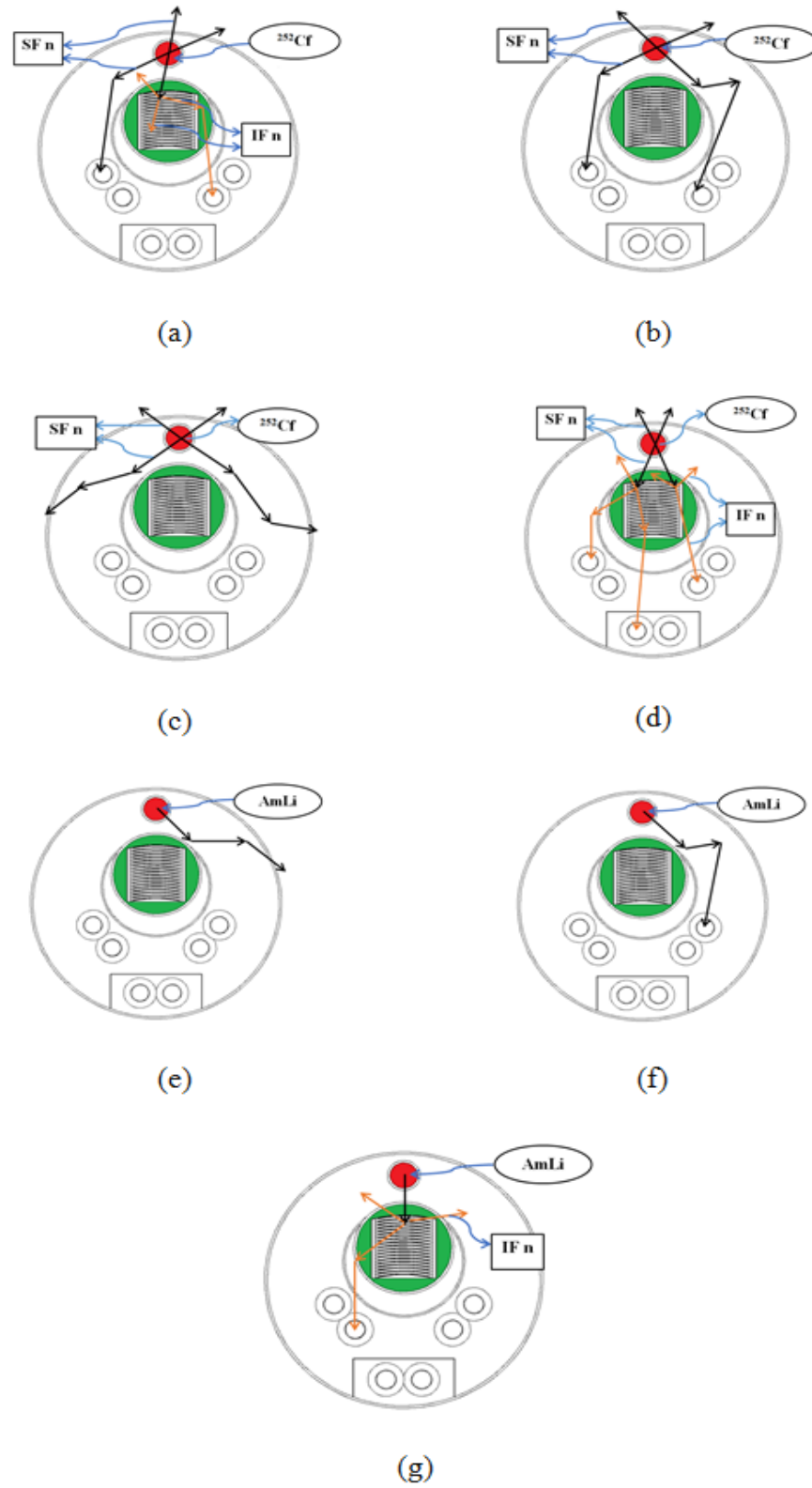
Figure 2-5: Possible neutron detection scenarios with active sources

2.11. UNCERTAINTY PROPAGATION

In radiation measurements, the total uncertainty in the measurement should account for uncertainties in both the source and background. In the AEFC coincidence measurements, background uncertainty comes from active source neutrons and room background neutrons. [8][6]

In case of the AEFC measurements, net singles and doubles are calculated as,

$$S_{net} = S_{Gross\ active} - S_{active\ background} \tag{18}$$

$$D_{net} = D_{gross\ active} - D_{active\ background} \tag{19}$$

Active background rates are combination of the room background and the background from the source with no fuel present:

$$S_{actve\ background} = S_{room} + S_{active\ source} \tag{20}$$

$$D_{actve\ background} = D_{room} + D_{active\ source} \tag{21}$$

The uncertainty in the active background singles and doubles count rates are given by:

$$\sigma^2_{S_{active\ background}} = \sigma^2_{S_{active\ source}} + \sigma^2_{S_{room\ background}} \tag{22}$$

$$\sigma^2_{D_{active\ background}} = \sigma^2_{D_{active\ source}} + \sigma^2_{D_{room\ background}} \tag{23}$$

The uncertainty in the net active singles and doubles count rates are given by:

$$\sigma^2_{S_{net}} = \sigma^2_{S_{active\ fuel}} + \sigma^2_{S_{background}} \tag{24}$$

3. MECHANICAL SYSTEM AND MEASUREMENT PROCUDERES

3.1. MECHANICAL DESIGN

Figure 3-1 provides a visual representation of the AEFC system. Picture on the right is a top view of the system in which location of six ^{3}He detector, an ion chamber, crescent shaped lead shielding, lead sleeve, fuel through hole, and interrogation source slot can be seen. The picture on the left shows side view of the system. This view shows the axial dimensions and location of the material.
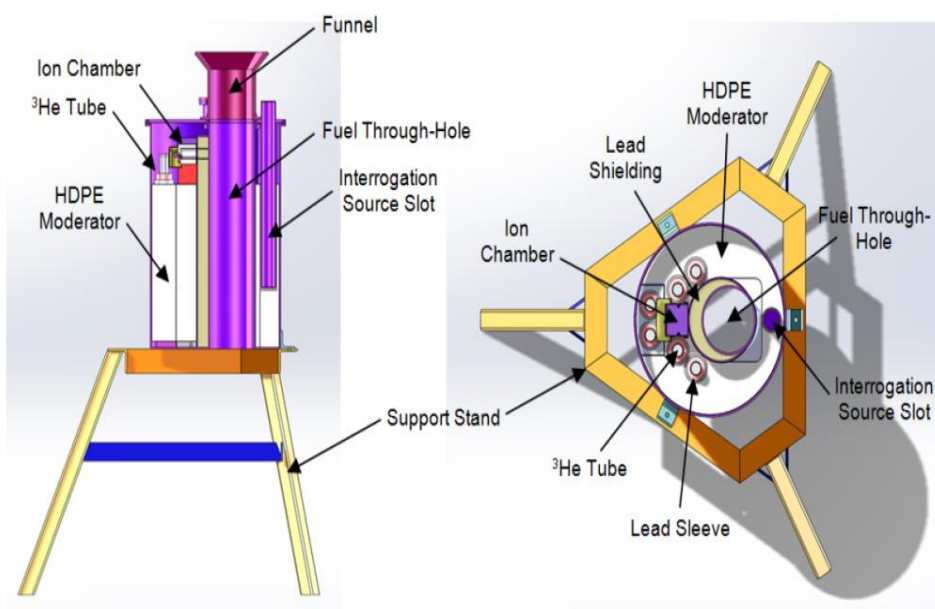
Figure 3-1: Mechanical design of the AEFC [5]

The AEFC system is an underwater measurement system, therefore it is watertight. It consists of 6 ^{3}He neutron detectors, a gross gamma-ray counter (ion chamber), high-density polyethylene (HDPE) moderator, and lead shielding inside the cylindrical stainless steel casing. It has a 117-mm diameter throughput-hole for fuel assemblies. A funnel placed on top of the throughput-hole helps guide assemblies to the desired measurement position. Interrogation source hole lies on the one side of the

throughput hole, whereas the neutron and gamma detectors are placed on the opposite side behind the crescent shaped lead shielding. Six boron-lined ^{3}He detector tubes at 4 atm of gas pressure are each surrounded by a 10-mm-thick lead sleeve and HDPE moderator. The ion chamber is positioned on top of the HDPE behind the lead shielding with a collimator hole. The wiring of AEFC such as from detectors, preamplifiers, and HVPS passes through the waterproof Tygon tube. The interrogation source is confined inside a HDPE holder and connected to a Teleflex cable. Interrogation source is moved into and out of the AEFC through a PVC guide tube that runs from the AEFC to the top of the spent fuel pool. [5] The Figure 3-2 is a top view of the AEFC when MTR fuel assembly is inserted inside the fuel through hole.
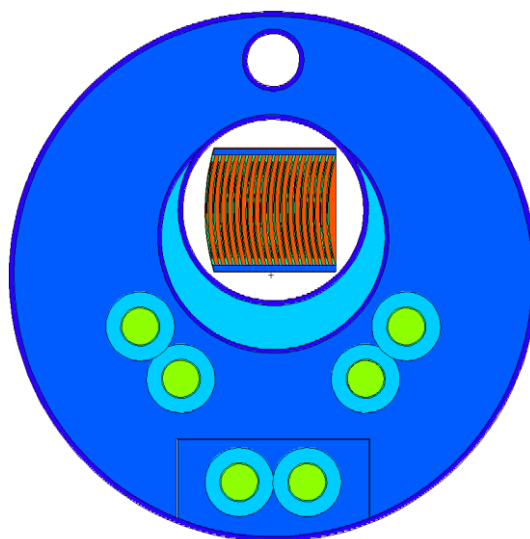
Figure 3-2: MTR assembly inside AEFC generated from MCNP plotter

3.2.   DATA ACQUISITION

AEFC was placed inside a water tank that had a water level of approximately 117 cm from the base of the water tank. High voltage (HV), pre-delay, and gate were set to 1680V, 4.5µsec, and 128µsec. Neutron data was collected in a JSR shift register. The shift register data was then collected in a laptop and analyzed in "Rates Only" mode using IAEA Neutron Coincidence Counting (INCC) software to obtain the singles and

doubles count rates. Although there is a gross gamma counter inside the AEFC system, gamma measurements were not performed. [5]

3.3.   EXPERIMENTAL MEASUREMENT METHODOLOGY

Since a complete fuel assembly scan was desired, the measurements were started by putting the 108 cm long MTR fresh fuel assembly (L-108) completely inside the fuel throughput hole such that the bottom of assembly touched the bottom base of water tank. ^{252}Cf, an active interrogation source, was placed inside the source slot. Since the L-108 fuel assembly was too long, a full assembly scan was not performed. As the top of the ^{3}He detector was at 80.34 cm from the base of the tank, only 80.34 cm of the fuel assembly could be scanned. With 25.34 cm length of ^{3}He detectors, center of theses detectors lies 67.67 cm above the base of the water tank. The starting point of scan of fuel assembly L-108 was at approximately 16.60 cm in the fuel active region. This implies that only approximately 44 cm of active fuel length out of 60 cm and 24 cm of bottom empty region could be scanned.

The fuel assembly has small holes approximately 3 cm below the top in an inactive region, which is often used to handle the fuel assembly by using either positioning jig or a string. In this experiment, a string was tied to the assembly using these holes. Since the movement of assembly was vertical, a hook of crane was placed some distance above the assembly. The hook of the crane was tied on both sides of a tank by using ratchet belt so that the hook location would remain fixed during the entire experiment. A pulley was designed by moving the string from the top of hook to the clamp attached on the side of the water tank top. A string was pulled to its maximum stretch while the assembly was still touching the base of the tank. A measuring stick was used to mark 3 cm apart 23 steps. 23 separate 1 minute measurements were recorded with the 3 cm increment each time from the base of the tank. The active region of a fuel assembly was pulled out of the AEFC and with this setup 5-minute background Count Rate of ^{252}Cf and AmLi active interrogation sources were recorded separately. One of the objectives of this experiment was to perform three-point scan of a fuel assembly, but the length of L-108, 108 cm, made it impossible to measure the top third of the assembly at the center point of the active region of the detectors. Therefore, only middle and bottom scans were performed for this type of assembly.

The assembly was raised 13.67 cm above the base by using the same marking method. By raising the assembly by 13.67 cm the center of assembly aligned with the center of ^{3}He detector. In this center position, 10 min measurements were recorded separately with ^{252}Cf and AmLi sources. To check on the sensitivity to the plate orientation, the assembly was rotated by 90 degrees and a 10 min measurement was recorded with the ^{252}Cf source at the mid-point configuration.

Next, the 108.26 cm long L-108 MTR fuel assembly was replaced by the 90.48 cm long O-187R MTR fuel assembly. The bottom of this type of MTR assembly has approximately 18 cm less inactive region, therefore with this type of fuel it was possible to make a 3-point scan in the AEFC. The middle point of the active region was at 31.32 cm above the base, while the top and bottom were 18 cm up and down axially from the middle point.

The same process was used to mark the string as was used in the case of assembly L-108. 10 minute measurements of top, middle and bottom of active fuel assembly were recorded with ^{252}Cf source, while the middle measurement with AmLi was performed overnight, approximately 13.3 hours. With ^{252}Cf source and fuel assembly rotated by 90 degrees, 10 minute measurements of middle part were recorded.

A separate measurement campaign was performed in which an aluminum fuel plate holder was fabricated to carryout measurements with varying ^{235}U mass. In this measurement campaign, a different ^{252}Cf source (A7869) with strength of 1.71E+05 n/s was used. Fuel plate configurations are shown in Figure 3-3.

| (a) 1 plate | (b) 8 plates | (c) 9 plates |
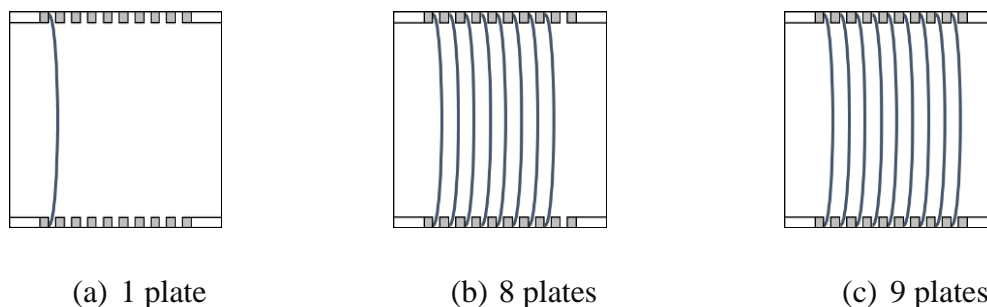
Figure 3-3: Varying fuel plates in a fuel holder

Once again the experiment started with the 20-minute measurement of the ^{252}Cf source to obtain a new ^{252}Cf background. The fuel plate holder was lowered into the water tank inside the AEFC fuel through hole. Three-point scan of the various numbers of fuel plates in a plate holder was performed. For middle measurement, axial center of fuel plates in the holder was aligned with the axial center of ^{3}He detectors. For top and bottom measurements, the fuel plates were shifted 18cm up and down respectively axially. Singles and doubles from 20 minute measurements were recorded.

3.4. MCNP SIMULATION METHODOLOGY

The MCNP set was created to replicate the experimental setup described in Section 3.3.

3.4.1. Full Assembly MCNP Setup. All MCNP6 simulations were carried out using a "full MTR assembly" as shown in Figure 3-4a. The schematic showing the "full assembly" setup with the AEFC detector system is shown in Figure 3-5. The axial setup shown in Figure 3-5(b) is referred to as the "midpoint" configuration, in which the base of the fuel assembly is 13.67 cm from the inner base of the tank. In this "midpoint" configuration, the midpoints of ^{3}He detectors in AEFC aligned with the midpoint of the fuel assembly. The following measurements were performed for the full assembly setup:

a. The Californium source was placed inside the source hole, and a measurement was performed using the "midpoint" configuration as shown in Figure 3-5(b).

b. A measurement was performed at 18 cm above the "midpoint" configuration.

c. Fuel assembly was lowered to the base of the water tank. Subsequently, 23 measurements with a 3 cm axial shift in the upward direction with each subsequent measurement took place.

d. A measurement was performed using the "midpoint" configuration as shown in Figure 3-5. The fuel assembly, however, was rotated 90 degrees in a counter-clockwise motion prior to the measurement occurring.

e. With the full assembly at mid-point configuration, measurements were performed with varying ^{235}U enrichments and varying fuel plates.

f. The ^{252}Cf source was replaced by AmLi source inside the source hole, and a measurement was performed using the "midpoint" configuration as shown in Figure 3-5(b).

Figure 3-4 and 3-5 are generated from the MCNP plotter. Figure 3-4 (a) represents full assembly, whereas Figure 3-4 (b) represents partial assembly. Figure 3-5 (a) provides the visual representation of the radial view, the source hole is colored red, and the fuel hole is colored green. Figure 3-5 (b) shows the "midpoint" configuration of MTR assembly inside the AEFC.
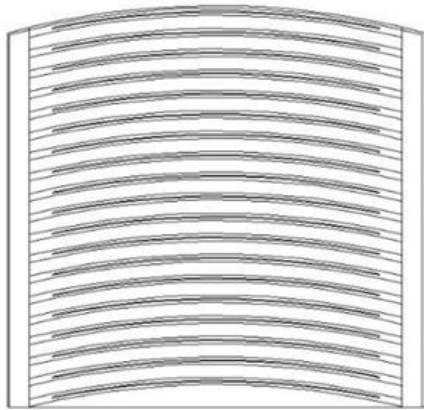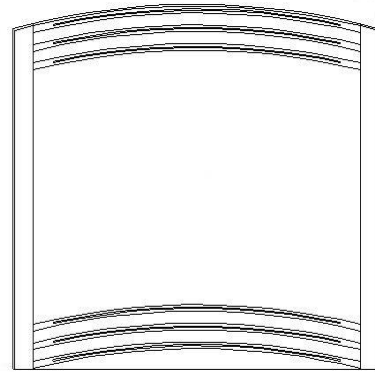
(a) MTR Full Assembly   (b) MTR Partial Assembly

Figure 3-4: Radial depiction of the "full" and "partial" MTR assemblies
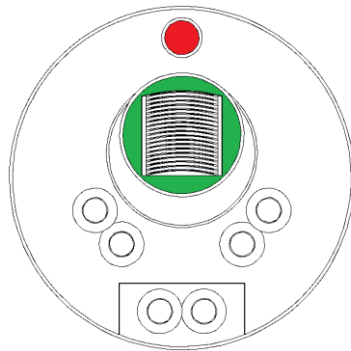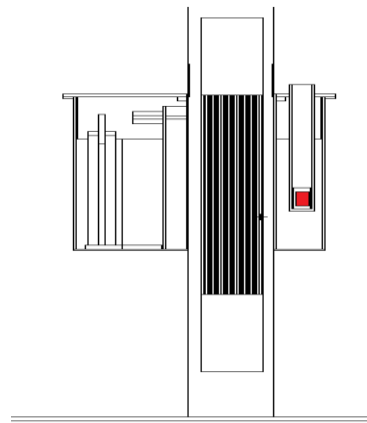
(a) Radial view   (b) Axial view

Figure 3-5: The combined MTR fuel assembly and AEFC experimental setup

3.4.2. Partial Assembly MCNP Setup. In the section of the experimental setup, all simulations were carried out using a "partial MTR assembly" as shown in Figure 3-4b. The following measurements were performed for the partial assembly setup:

a. Step a of Section 3.4.1 was repeated for the partial assembly.

b. Measurements were performed at 18 cm above and below the "midpoint" configuration to obtain a top and bottom measurements.

d. Step d of Section 3.4.1 was repeated for the partial assembly.

e. Step f of Section 3.4.1 was repeated for the partial assembly.

4. FRESH MTR FUEL, MATERIAL USED, AND SOME KEY DIMENSIONS

4.1. FUEL ASSEMBLY L-108

- Fuel assembly total length of 108.27 cm
- Active length of 60 cm in the middle of the assembly
- 24.13 cm of empty region on both sides of the assembly

4.2. FUEL ASSEMBLY O-187R

- Total length of 90.48 cm
- Active length of 60 cm
- 24.13 cm of empty region on top of the assembly
- 6.35 cm of empty region at the bottom of the assembly

4.3. MATERIALS USED

The following materials were used to complete AEFC fresh MTR fuel experiments at LANL:

- Clean AEFC system
- Water tank in high bay
- Crane in high bay for moving AEFC system
- ^{252}Cf (A7866)- 45,670 n/s
- ^{252}Cf (A7869)- 170,695 n/s
- AmLi (N-165) – 37,940 n/s
- JSR-15 shift register
- Laptop with INCC
- L-108 and O-187R

4.4. KEY DIMENSIONS

a) Height of the AEFC is 112.1 cm from top of the funnel to the inside base of the water tank
b) Water depth of 117 cm
c) Center of He-3 detector to the base of the water tank is 67.67cm
d) Position of interrogation source at 67.67 cm from the base
e) Diameter of fuel through hole is 11.7 cm
f) Length of ^{3}He detector is approximately 25.34 cm

In the Figure 4-1, part a provides the visual representation of the AEFC used in the experiments, part b shows partial MTR fuel assembly loaded with only 6 fuel plates, part c shows AEFC underwater loaded with MTR fuel assembly, and part d shows AEFC internal components.

(a) AEFC System used in the experiments [18]
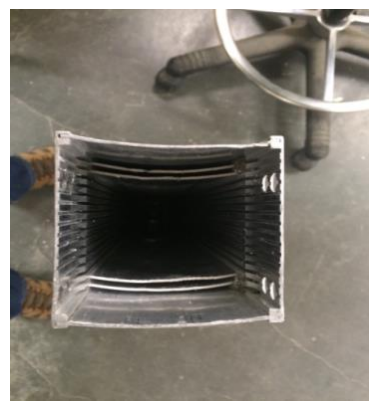
(b) MTR half assembly O-187R

(c) AEFC System inside the water with MTR Fuel assembly from previous experiment [19]
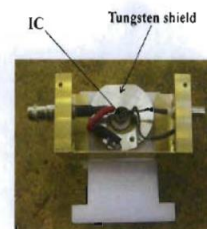
(d) AEFC internal components [19]

Figure 4-1: AEFC components and the fresh MTR fuel assembly

5. RESULTS AND ANALYSIS

Since the source strengths of AmLi (N-165) and ^{252}Cf were approximately 37,940 n/s and 45,670 n/s, respectively, at the time of experiments on 9/21/2016, the source strength of ^{252}Cf is 1.204 times higher than the AmLi source. While comparing ^{252}Cf and AmLi measurement results, all ^{252}Cf measurement count rates are normalized to the AmLi count rates by dividing ^{252}Cf count rates by 1.204. The source strength of second ^{252}Cf (A7869) source was approximately 170,695 n/s, which is 3.738 times the strength of first ^{252}Cf (A7-866) source. The measurement results with A7-869 source were normalized to the A7-866 source strength by dividing A7869 results by 3.738. Since $3 *$ σ uncertainty is considered acceptable confidence interval, the error bars in all figures in this section represent $3 * \sigma$ from the measured or simulated values. The efficiency of the system with only active source in air is approximately 2.5% and 5.35% when the active source is placed inside the source hole and fuel hole respectively. In water, the efficiency changes to approximately 1% when the source in inside the source hole and 5.88% when the source is inside the fuel hole. The efficiency reduced in water when the active source was placed inside source hole due to over moderation of neutrons.

The results and analysis section starts with the benchmarking of full and partial assemblies. Then, the AEFC calibration is presented. The calibration section will contain singles and doubles count rates versus mass of ^{235}U. Then, a section will show the comparison of singles and doubles count rates due to ^{252}Cf and AmLi sources with a discussion of the boost in doubles rate due to TCIF effect when ^{252}Cf source is used.

5.1. FULL ASSEMBLY (L-108) BENCHMARK

The L-108 MTR fresh fuel assembly was measured in 3 cm increments along the active length axially. The singles and doubles from the experiment are compared with singles and doubles from the MCNP simulation in Figure 5-1. When the fuel assembly L-108 is 0 cm above the base of a water tank, the centers of the ^{3}He detector and interrogation source are aligned at 16 cm below active fuel region from the top. Therefore, only 44 cm of active region can be scanned using the present stand. Figure 5-1 shows singles and doubles count rate drop after the assembly was raised 36 cm above the

base, and at approximately 44 cm above the base count rates are halved from the peak rates. The interrogation source is moderated in the poly and water, and the fuel assembly is inserted inside the AEFC in an axial direction inside the fuel through hole as shown in Figure 3-5(b). Therefore, neutrons in the middle point measurement will not only come from the exact middle point of an active fuel region but also from some length up and down axially.
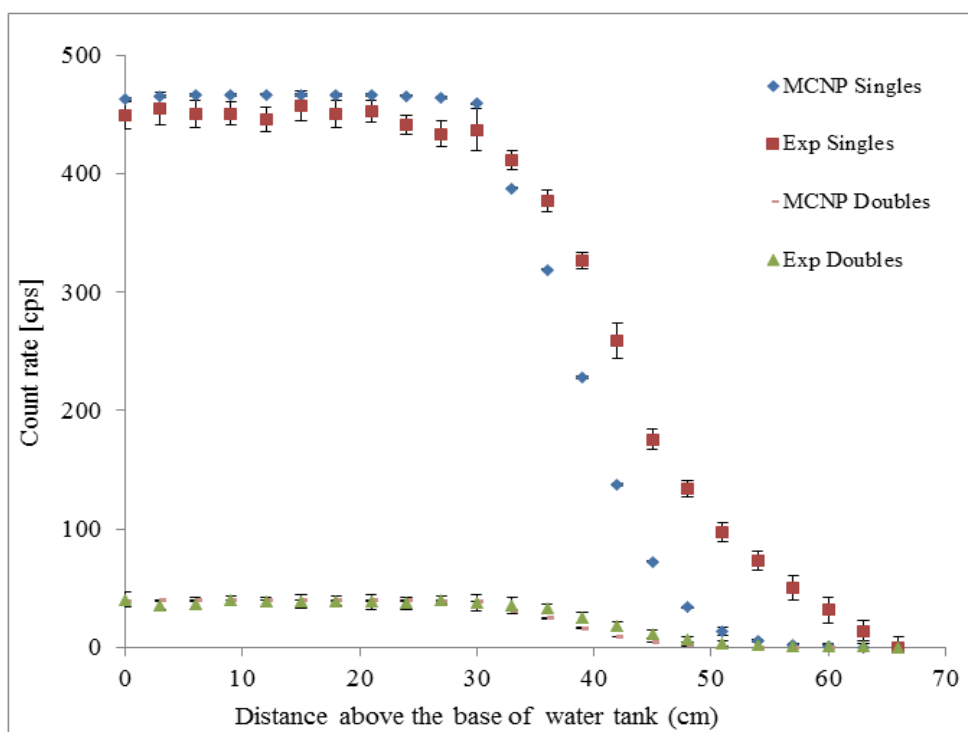
Figure 5-1: L-108 scan with ^{252}Cf SF source

The singles and doubles profiles are flat from 0 cm to 33 cm in this region because there is enough active fuel region on either side in axial direction of the point of measurement. After reaching 36 cm increment, both singles and doubles started decreasing, while at 44 cm increment the count rates are dropped to half of the maximum.

It is difficult to differentiate experimental and MCNP net doubles count rates in Figure 5-1, therefore Figure 5-2 represents comparison of experimental and MCNP net doubles count rates. MCNP singles and doubles rates agree with the experimental singles

and doubles rates within 5% and 4%, respectively up to the 36-cm increment measurement point. After 36 cm of measurements, MCNP and experimental singles and doubles start diverging. In this region, experimental singles and doubles are higher than MCNP. The reasons for this divergence could be many, such as no room background in MCNP results which has a larger effect in this region due to the decreased count rate. The results are diverging at the end of fuel assembly, where there is very small amount of fuel meat in the line of sight of the source and the Al end structure is increasing.
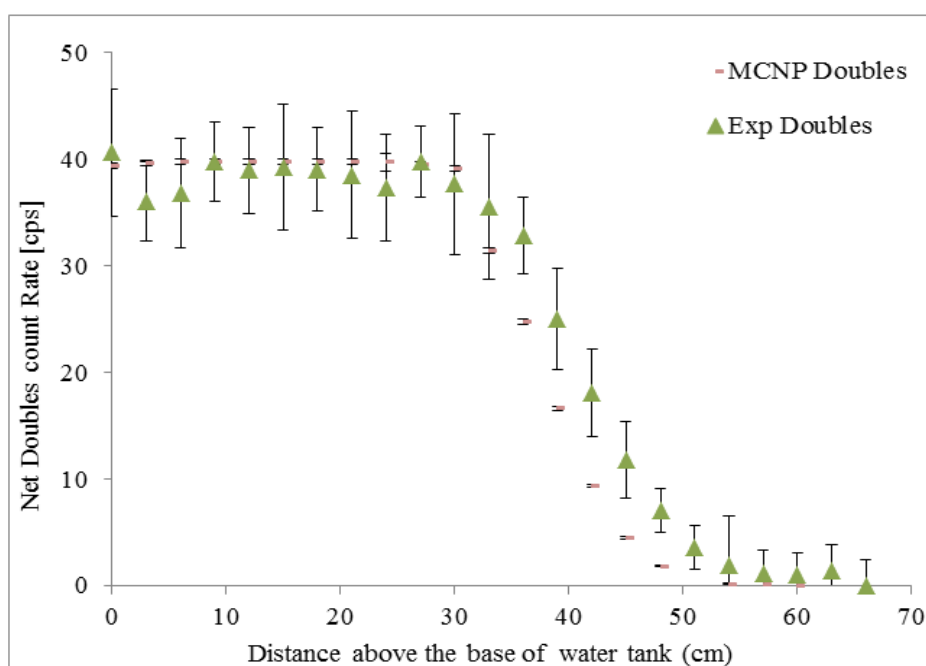
Figure 5-2: Assembly L-108 net doubles count rates

The MCNP results closely matched the experimental results for the two-point scan of the full assembly. The mid and bottom point measurements are 13.67 cm and 31.67 cm above the bottom of the active region of the fuel; the MCNP singles and doubles count rates agree with the experimental singles and doubles count rate within 5% for singles and 4% for doubles at these points. The Figure 5-3 and 5-4 show the experimental and MNCP comparison of singles rates and doubles rates of 2-point scan of the full assembly L-108.
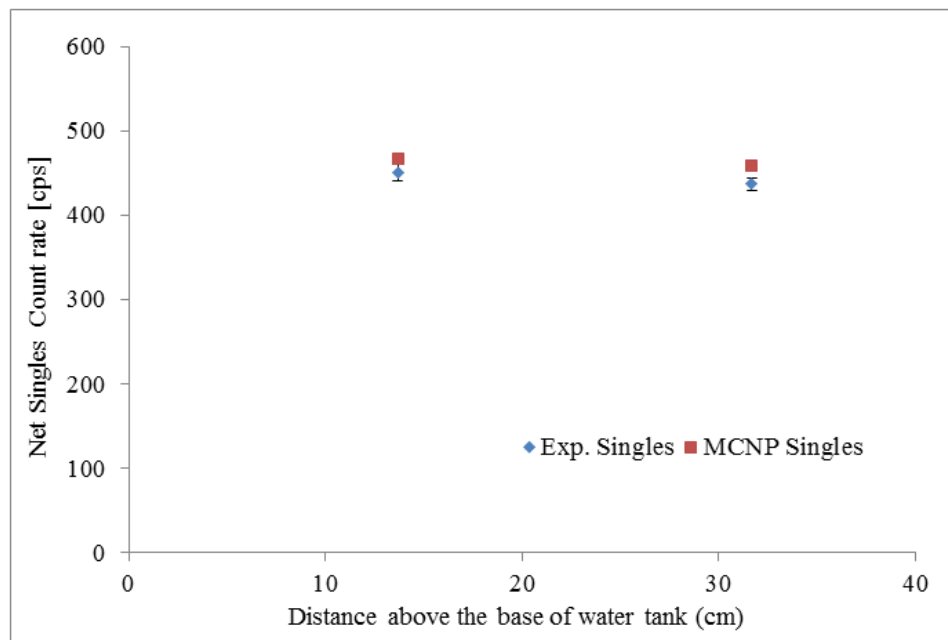
Figure 5-3: Singles results comparison of two-point scan of full assembly (L-108)
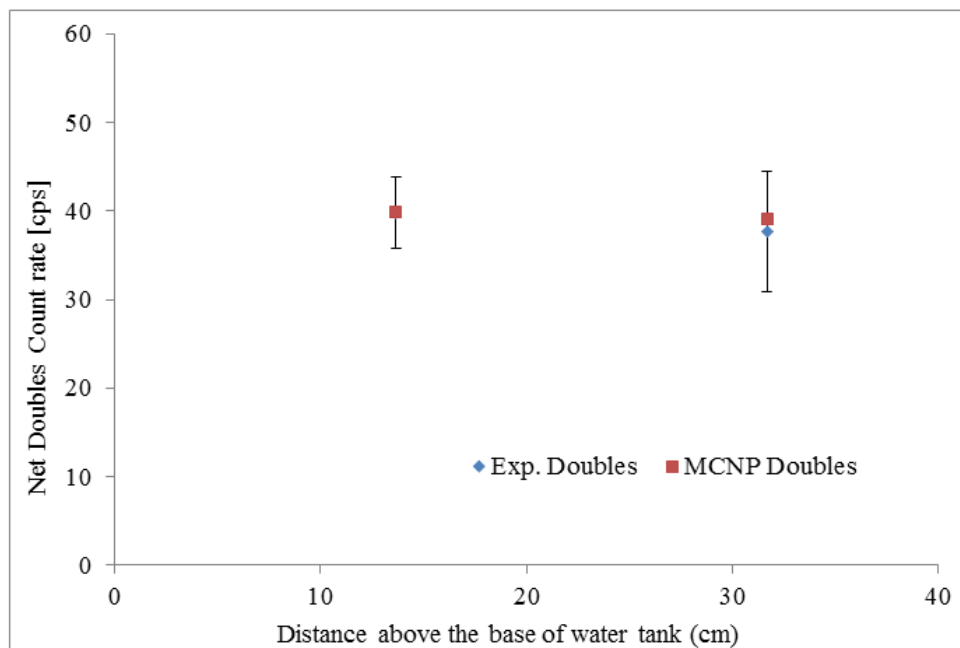
Figure 5-4: Doubles results comparison of two-point scan of full assembly (L-108)

5.2.   PARTIAL ASSEMBLY (O-187R) THREE-POINT SCAN

A three-point scan was also taken of the partial assembly, O-187, with only six fuel plates. The net singles and doubles count rates, or count rates with active background subtracted, are given in Figures 5-5 and 5-6. In these figures, the experimental net count rates are also compared with the MCNP net count rates.
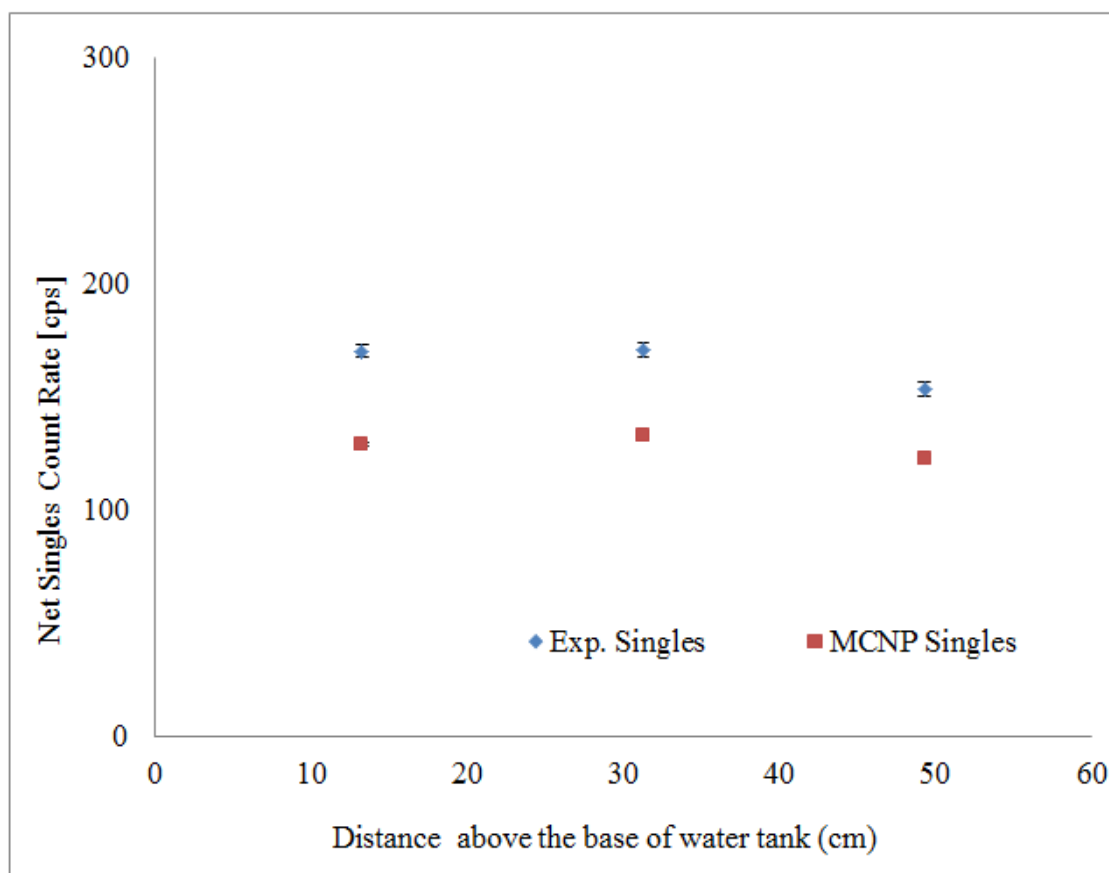
Figure 5-5: Three-point scan singles count rates of partial assembly

Figure 5-5 and 5-6 show benchmarking of partial assembly in which MCNP singles are within 20-25% agreement while doubles are within 3% agreement with experimental results. The partially loaded assembly has larger uncertainties that are related to the large water gaps in the plate configuration.
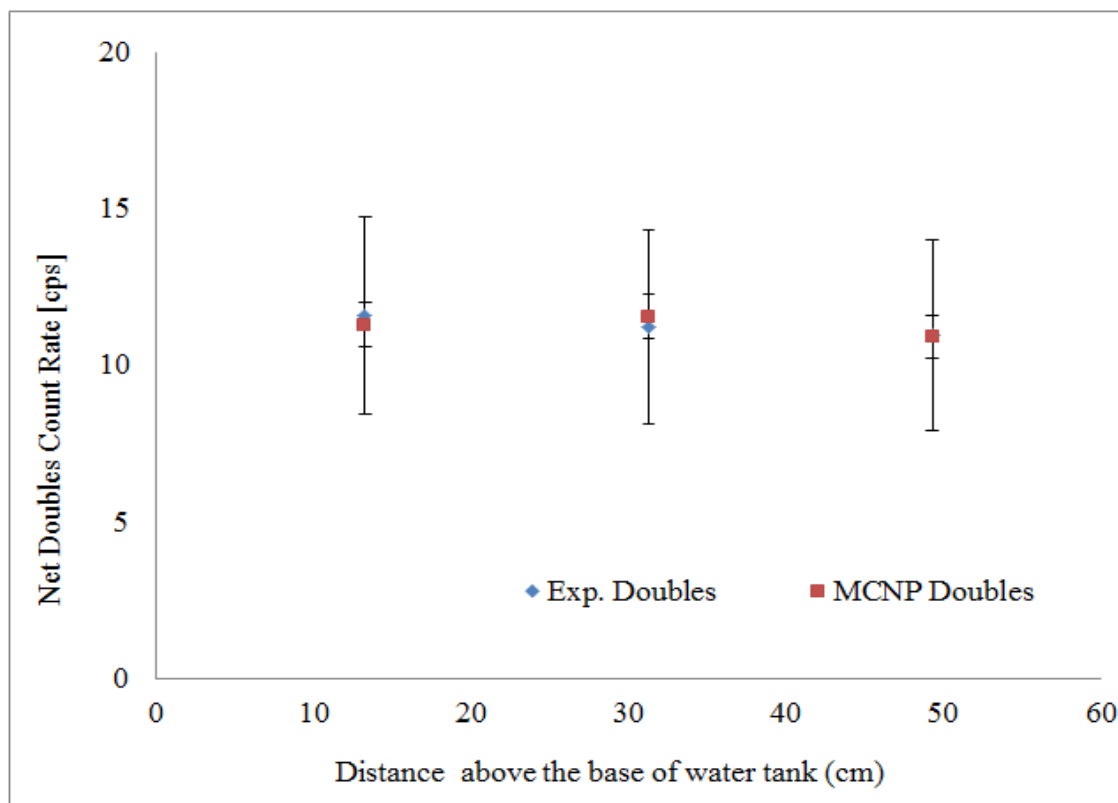
Figure 5-6: Three-point scan doubles count rates of partial assembly

5.3.   AEFC CALIBRATION

Figures 5-7 and 5-8 show comparisons of MCNP and experimental net singles and doubles count rates versus residual fissile mass (^{235}U) in the fabricated fuel plate holder varying from 0 plates to 9 plates, partial L-108 assembly varying fuel plates from 4 to 19. A full MTR assembly was simulated with varying enrichment from 19 to 93.5 percent. The case with variable enrichment is expected to have a different curvature because of the increase in neutron self-shielding with ^{235}U mass. Measurements were taken with the midpoint of the assemblies aligned with the midpoint of the active region of the ^{3}He detectors axially. The experimental points below 150 g of uranium are from the fabricated fuel plate holder and the point above 200 g of uranium is from the L-108 assembly. In all cases, the active background is subtracted.
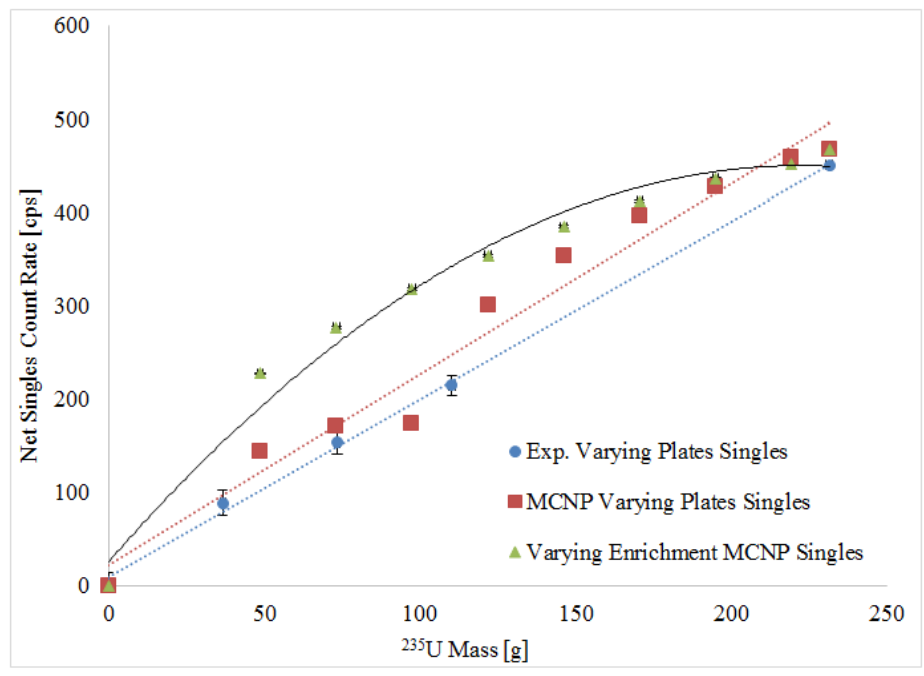
Figure 5-7: Calibration of singles count rates versus residual fissile mass of ^{235}U
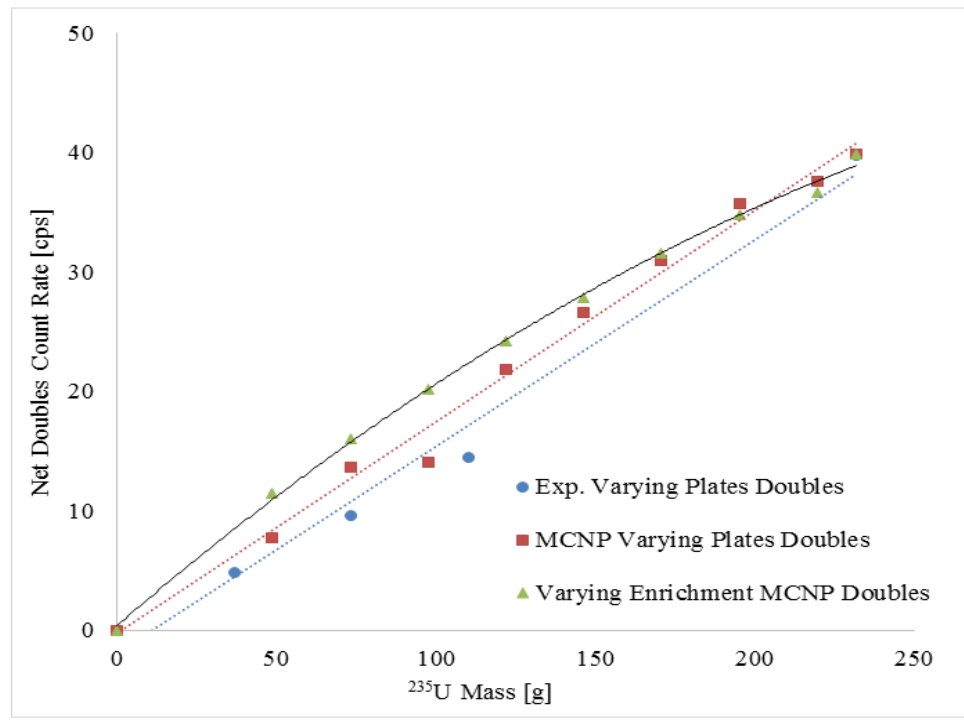
Figure 5-8: Calibration of doubles count rates versus residual fissile mass of ^{235}U

To verify residual fissile mass using an active interrogation source is one of the primary objectives of this research. The figure shows count rates change in two different scenarios, (1) change in count rates vs residual fissile mass when two fuel plates are removed in each steps. In this scenario, the ^{235}U enrichment remains the same while residual fissile mass changes due to the removal of fuel plates. This will cause increased moderation of neutrons from the active source or the IF. Also, in this case ^{238}U fraction remains the same, around 7%, which has a negligible effect. The second scenario (2) is a change in count rates vs residual fissile mass when enrichment is changed. This case is more realistic to the measurements for safeguards for the verification process. In this scenario, the number of fuel plates remains the same but residual fissile mass changes. Each time the enrichment decreases, ^{238}U fraction increases. When ^{235}U mass decreases, there is less IF resulting in lower count rates. In Figures 5-7 and 5-8, the counting rates with varying enrichment are higher compared to the constant enrichment, because the increasing ^{238}U fraction dilutes the ^{235}U density resulting in less thermal-neutron self-shielding. The self-shielding is mostly due to the ^{235}U in HEU fuels, while in LEU thermal-neutron absorption is mostly by the ^{238}U. At 93% enrichment both cases have the same count rates because the two setups (varying fuel plate number and varying enrichment) are the same for a full assembly. In the constant enrichment but varying fuel plates configuration, each time the fuel plates are removed from the assembly a large water gap is created between the fuel plates, which causes over moderation of IF or active source neutrons.

5.4.   COMPARISON OF ^{252}Cf AND AmLi NEUTRON SOURCES

Additional fuel assembly configurations were considered in MCNP simulation space as they could not be constructed in the lab with the experimental resources available. A three-point scan of a set of simulated assemblies with varying numbers of fuel plates from 4 to 19 was conducted in MCNP and compared to the average of the three points. The MCNP results are given in Figures 5-9 to 5-12 for both AmLi and ^{252}Cf.

Figures 5-9- 5-12 show the comparison of singles and doubles count rates of three-point scan with the average of scan in simulation space. Since the fuel under investigation was fresh fuel, it had uniformly distributed ^{235}U content. Thus, top, middle, and bottom measurements count rates are very close to each other. If instead the fuel

under investigation was burned/used fuel, we could have seen higher count rate in top and bottom while a relatively low count rate in the middle due to the higher residual fissile mass remaining at the ends compared to the middle. MCNP results show that for the same fissile residual mass, the normalized singles count rates per source neutron with AmLi are approximately 20 percent higher than with ^{252}Cf, while normalized doubles count rates are around 30 percent lower.

The ^{235}U mass change in Figures 5-9 to 5-12 was simulated by removing fuel plates from the assembly with the plates being removed from the outside and working inward towards the center. The water moderation of the neutrons has an impact on the shape of the response curves for the singles and doubles rates. Both the AmLi and the ^{252}Cf have the same response shapes for the doubles and singles rates. These response curves are specific to the plate removal procedure.

In Table 5-1, experimental results of full assembly show that the singles are higher and doubles are lower by approximately 20 percent and 16 percent respectively with AmLi compared to the results with ^{252}Cf. In the case of partial assembly (O-187R), the singles count rate is approximately 16 percent higher with AmLi while doubles count rate is around 12 percent higher with ^{252}Cf.
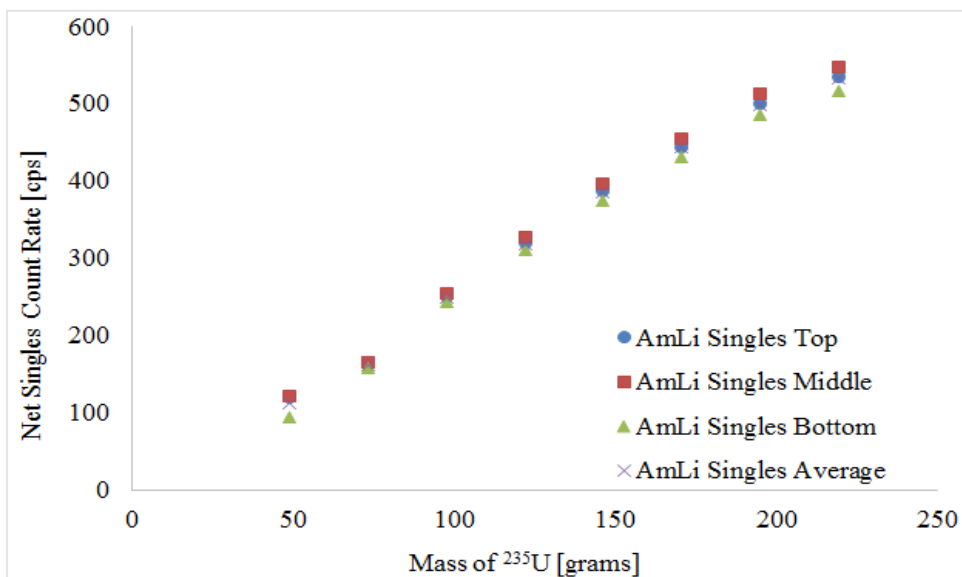
Figure 5-9: MCNP three-point singles calibration with AmLi source
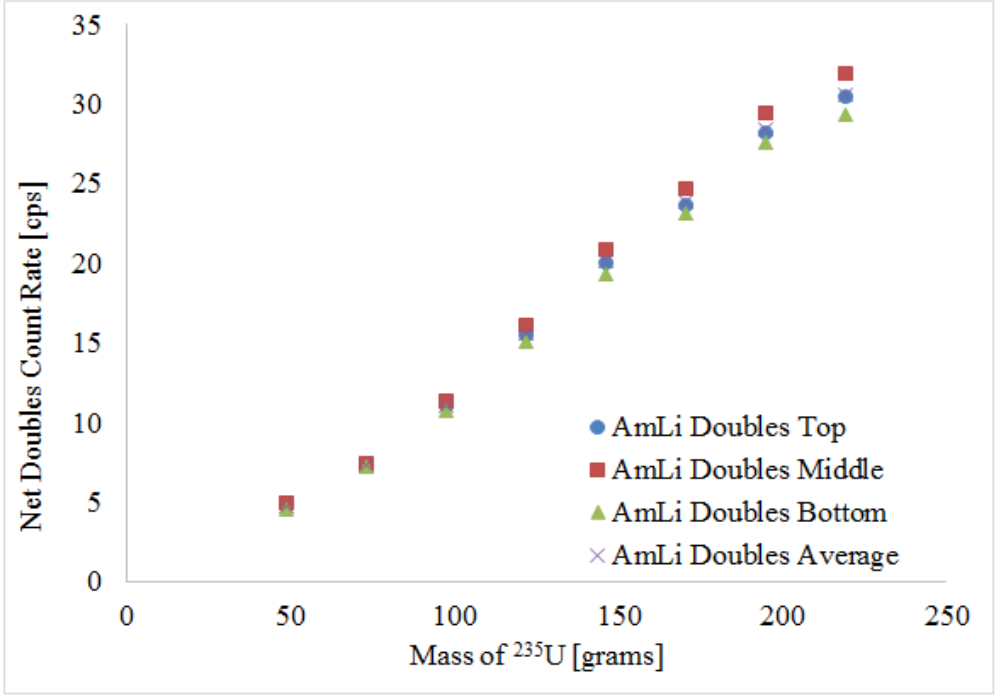
Figure 5-10: MCNP three-point doubles calibration with AmLi source
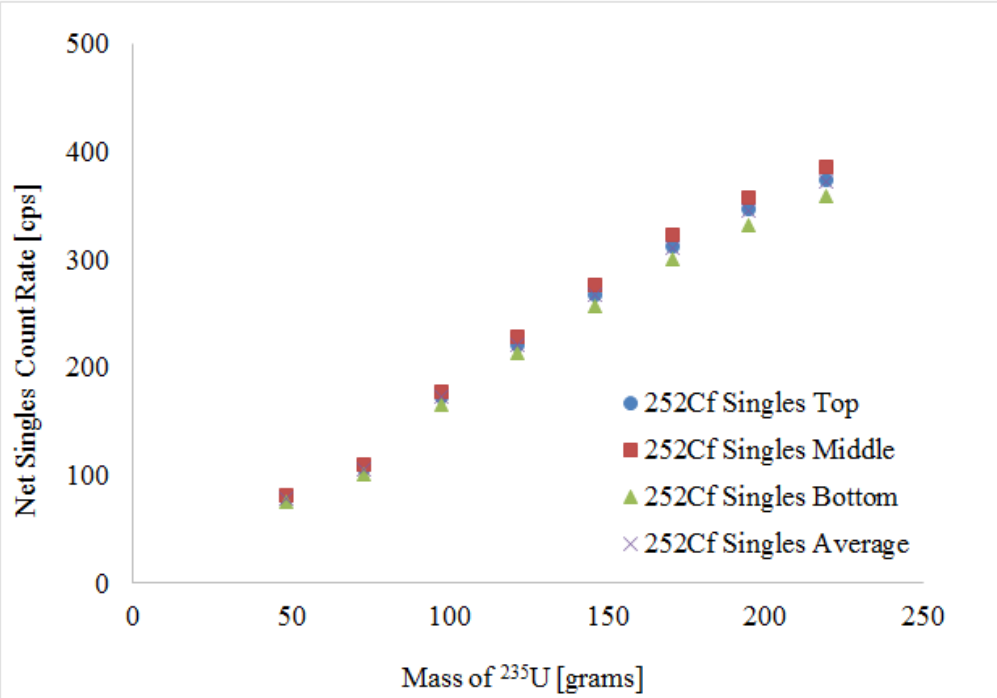
Figure 5-11: MCNP three-point singles calibration with ^{252}Cf source
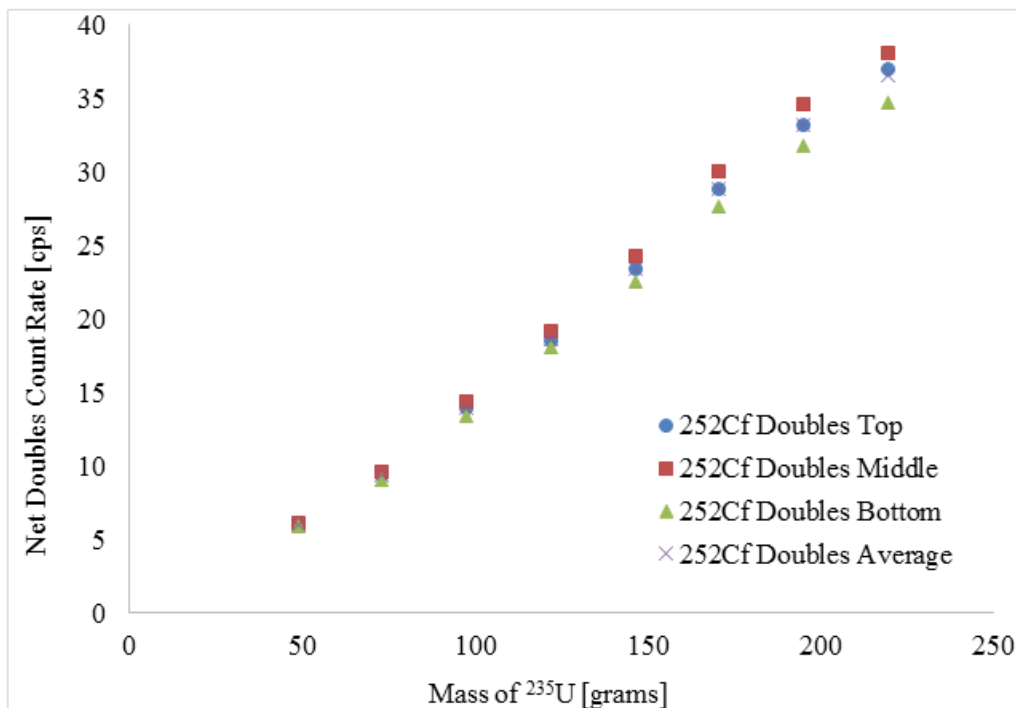
Figure 5-12: MCNP three-point doubles calibration with ^{252}Cf source

Table 5-1: Count rates comparison in full assembly and partial assembly

Full Assembly results normalized to AmLi strength & 600 sec counting time			
AmLi		^{252}Cf	
S	D	S	D
451.89±1.14	27.23±0.35	377.22±0.79	32.18±0.37
Partial Assembly results normalized to AmLi strength & 600 sec counting time			
AmLi		^{252}Cf	
S	D	S	D
164.65±0.84	8.22±0.23	142.12±0.85	9.34±0.28

5.5. ^{252}Cf RATES COMPARISON

One of the objectives of this research was to investigate the effects of change in geometry of fuel assembly to the singles and doubles count rates. Mid-point configuration measurements were performed with the assembly rotated 90 degrees along

with the original configuration described in Section 5.1 and 5.2. Table 5-2 shows count rate comparisons between an original configuration mid-point measurement and the mid-point measurement with fuel assembly rotated by 90 degrees with ^{252}Cf source. In the case of full assembly, singles and doubles count rates changed by 5.18% and 3.52% respectively when the fuel assembly was rotated by 90 degrees. In the case of partial assembly, the change was 9.7% and 1.96% respectively for singles and doubles count rates.

Table 5-2: Effects of change in geometry of the fuel assembly in the count rates

	Singles	Doubles
Exp Original Configuration (FA)	450.71±3.41	39.78±1.34
Exp 90 deg rotated Configuration (FA)	427.35±1.95	38.38±0.69
Exp Original Configuration (PA)	170.54±1.025	11.21±0.334
Exp 90 deg rotated Configuration (PA)	154.07±1.621	10.99±0.424

The results in Table 5-2 show that by changing the geometry of FA by 90 degrees the singles rate changed by approximately $7 * \sigma$ value of the original configuration, while doubles count rate is within $2 * \sigma$ value. In the PA, singles rate changed by approximately $16 * \sigma$, while doubles rate changed by less than 1σ. The singles rate clearly has a bigger change compared to the doubles rate which changed marginally. This analysis is based on only two data points therefore further more data points are needed to confirm the effect of geometry in count rates. However, during the verification measurements this change in singles rate needs to be taken into account.

5.6.   TIME CORRELATION EVALUATION

Table 5-3 shows the comparison of singles and doubles IF rates per source strength (i.e. count rates with active background subtracted) with AmLi and ^{252}Cf active interrogation sources.

Table 5-3: Experimental count rates per source strength

	AmLi, N-165	^{252}Cf, A7-866
Singles IF/Source	1.19E-02	9.70E-03
Doubles IF/Source	7.18E-04	8.36E-04

When source strengths of active sources AmLi and ^{252}Cf are normalized, IF rates provide interesting results. The singles IF rate per source neutron with AmLi is 1.228 times the singles IF rate due to ^{252}Cf, because the lower energy of neutrons emitted from AmLi source have more chances to get absorbed into the fuel element. The doubles IF rate per source neutron with ^{252}Cf is 1.176 times the doubles IF rate due to AmLi, because the ^{252}Cf source produces time correlated neutrons. If the TCIF effect of ^{252}Cf source could be eliminated, AmLi source would have resulted in higher singles and doubles count rates. Table 5-4 shows net doubles IF to net singles IF ratios for the AmLi and ^{252}Cf sources.

Table 5-4: Experimental doubles IF to singles IF ratio

Source	Doubles IF/Singles IF
AmLi, N-165	6.03E-02
^{252}Cf, A7-866	8.62E-02

Net doubles to net singles ratio with ^{252}Cf is 1.431 times higher than the net doubles to net singles ratio with AmLi source. With AmLi source, on average, 16.595 singles are needed for each doubles count, but with ^{252}Cf only 11.596 singles are needed for each doubles count. The same effect is evident in MCNP as shown in Tables 5-5 and 5-6.

Table 5-5: MCNP count rates per source strength

	AmLi, N-165	^{252}Cf, A7-866
Singles IF/Source	1.14E-02	9.88E-03
Doubles IF/Source	6.91E-04	1.01E-03

Table 5-6: MCNP Doubles IF to singles IF ratio

Source	Doubles IF/Singles IF
AmLi, N-165	6.02E-02
^{252}Cf, A7-866	1.01E-01

MCNP simulation results in Table 5-5 and 5-6 show similar results to the experimental results shown in Tables 5-3 and 5-4. Here, net doubles to net singles ratio with ^{252}Cf is 1.7 time higher than with AmLi source.

6. SUMMARY AND CONCLUSION

The objective of this research was to evaluate the response of the AEFC for use in the verification of MTR type fuel assemblies where both ^{252}Cf and AmLi neutron sources were used to interrogate the fuel assemblies. MTR type fuel assemblies with variable ^{235}U loadings were measured to benchmark MCNP simulations. The experimental results were used to generate count rates versus residual fissile mass calibration curves with the ^{252}Cf active source. We investigated the effects of change in fuel assembly geometry and showed the boost in doubles count rates (coincidence rates) when ^{252}Cf is used in lieu of AmLi active source.

The MCNP simulation results show that the benchmarking of singles and doubles count rates of full assembly were within 5% and 4%, respectively. Sources of error in the MCNP simulation may include exclusion of impurities, HDPE volume, air gap, SS volume, lead volume, boron thicknesses, and finally the fuel assembly. However, this MCNP model could be used in the future AEFC experiment verifications.

Section 5.5 shows higher IF singles and lower IF doubles per source neutron with AmLi compared to ^{252}Cf. IF doubles to IF singles ratio is 1.431 times higher when ^{252}Cf is used compared to the AmLi source. This results from the boost in doubles count rate when ^{252}Cf is used. The reason behind this is that the time correlated SF neutrons emitted by ^{252}Cf source, which causes time correlated IF events in the fuel, result in additional coincident events from neutrons in the same fission chain. Even though the lower energy of AmLi neutrons have a higher probability to get absorbed into the fuel assembly compared to the higher energy neutrons from ^{252}Cf, the results show higher coincidence count rates with ^{252}Cf source. This indicates that the boost in the doubles rate with ^{252}Cf source is due to the time correlations in the SF of the ^{252}Cf.

For future work, an experimental calibration of the AEFC with the fresh fuel containing higher percentage of ^{238}U on average and varying ^{235}U enrichment could be performed. The AEFC could be calibrated with fresh fuel rods containing various concentrations of GdO_3 poison rods to simulate fission product absorption.

APPENDIX A.

EXPERIMENTAL MEASUREMENT RESULTS

MTR Assembly L-108 Scan with ^{252}Cf

Distance	singles	singles error	Doubles	Doubles error
0	874.417	3.477	41.538	1.953
3	878.633	4.340	43.967	1.245
6	884.633	3.664	39.383	1.700
9	879.983	2.912	40.167	1.257
12	880.450	3.138	43.117	1.338
15	875.617	4.111	42.317	1.969
18	886.867	3.580	42.667	1.311
21	880.183	2.752	42.417	1.989
24	882.283	2.330	41.867	1.670
27	870.617	3.296	40.683	1.112
30	863.067	5.674	43.100	2.211
33	866.633	2.320	41.033	2.267
36	841.250	2.633	38.900	1.204
39	806.517	1.939	36.167	1.585
42	756.617	4.888	28.317	1.368
45	688.500	2.600	21.483	1.192
48	605.350	1.791	15.175	0.671
51	563.817	2.328	10.417	0.681
54	527.500	2.196	6.956	1.542
57	503.133	3.125	5.283	0.767
60	480.117	3.408	4.433	0.696
63	461.467	2.394	4.383	0.824
66	443.933	2.732	4.733	0.824

MTR Assembly L-108 Scan with ^{252}Cf subtracted with ^{252}Cf background

Distance	singles	singles error	Doubles	Doubles error
0	444.68	3.7226911	38.201	1.980186355

3	448.896	4.53921799	40.63	1.245
6	454.896	3.89792201	36.046	1.7
9	450.246	3.20135034	36.83	1.257
12	450.713	3.40821713	39.78	1.338
15	445.88	4.3207894	38.98	1.969
18	457.13	3.81907057	39.33	1.311
21	450.446	3.05653464	39.08	1.989
24	452.546	2.6828716	38.53	1.67
27	440.88	3.55422509	37.346	1.112
30	433.33	5.82779341	39.763	2.211
33	436.896	2.67419147	37.696	2.267
36	411.513	2.94984559	35.563	1.204
39	376.78	2.35130198	32.83	1.585
42	326.88	5.06571259	24.98	1.368
45	258.763	2.92042805	18.146	1.192
48	175.613	2.23082518	11.838	0.671
51	134.08	2.68113483	7.08	0.681
54	97.763	2.56735584	3.619	1.542
57	73.396	3.39625161	1.946	0.767
60	50.38	3.65832803	1.096	0.696
63	31.73	2.73863762	1.046	0.824
66	14.196	3.03853978	1.396	0.824

^{252}Cf Bkg and AmLi Bkg

	Singles	Singles Error	Doubles	Doubles Error
252Cf	429.737	1.330	3.337	0.327
AmLi	227.257	0.801	0.020	0.154

MTR Assembly L-108 two-point scan with ^{252}Cf and middle scan with AmLi

	Singles	Singles Error	Doubles	Doubles Error
Mid scan-^{252}Cf	872.713	1.272	41.538	0.592
Mid scan-^{252}Cf / rotated 90 deg	857.085	1.420	41.720	0.613
Bottom-^{252}Cf /18cm	808.373	1.272	39.743	0.558
Mid scan-AmLi	679.148	1.135	27.25	0.348

MTR assembly L-108 two-point scan with ^{252}Cf and middle scan with AmLi minus Bkg

	Singles	Singles Error	Doubles	Doubles Error
Mid scan-^{252}Cf	442.976	1.840	38.201	0.676
Mid scan-^{252}Cf / rotated 90 deg	427.348	1.945	38.383	0.694
Bottom-^{252}Cf /18cm	378.636	1.840	36.406	0.647
Mid scan-AmLi	451.891	1.389	27.23	0.380

MTR assembly O-187R three-point scan and middle scan with AmLi

	Singles	Singles Error	Doubles	Doubles Error
Bottom scan-^{252}Cf	583.245	1.019	14.282	0.368
Middle scan-^{252}Cf	600.278	1.025	14.550	0.334
Top scan-^{252}Cf	599.930	1.047	14.913	0.302
Mid scan-AmLi	391.912	0.094	8.241	0.026
Mid scan- ^{252}Cf rotated 90 deg	583.808	0.928	14.325	0.424

MTR assembly O-187R three-point scan and middle scan with AmLi minus Bkg

	Singles	Singles Error	Doubles	Doubles Error
Bottom scan-^{252}Cf	153.508	1.675	10.945	0.492

Middle scan-^{252}Cf	170.541	1.679	11.213	0.467
Mid scan-AmLi	164.665	0.806	8.221	0.156
Mid scan- ^{252}Cf rotated 90 deg	583.808	0.928	14.325	0.424

APPENDIX B.

MCNP SIMULATION RESULTS

MCNP simulation raw results of MTR Assembly L-108 with ^{252}Cf source

Distance	singles	singles error	Doubles	Doubles error
0	878.33	0.13	49.20	0.61
3	880.17	0.13	49.32	0.61
6	881.46	0.13	49.45	0.61
9	881.93	0.13	49.49	0.61
12	882.33	0.13	49.57	0.61
15	882.34	0.13	49.47	0.61
18	881.85	0.13	49.45	0.61
21	881.44	0.13	49.63	0.61
24	879.32	0.13	49.16	0.61
27	874.16	0.13	48.68	0.62
30	863.84	0.13	47.57	0.63
33	841.03	0.13	44.54	0.64
36	798.51	0.13	39.51	0.67
39	730.73	0.14	31.79	0.74
42	642.38	0.14	22.64	0.87
45	560.24	0.15	14.37	1.05
48	499.96	0.16	8.56	1.32
51	463.84	0.16	5.61	1.55
54	445.28	0.17	4.15	1.76
57	437.47	0.17	3.67	1.85
60	433.86	0.17	3.52	1.89
63	432.05	0.17	3.48	1.9
66	432.18	0.17	3.48	1.9

MCNP results of MTR Assembly L-108 with ^{252}Cf source minus ^{252}Cf background

Distance	singles	singles error	Doubles	Doubles error
0	446.69	0.16	45.73	1.26

3	448.53	0.16	45.84	1.25
6	449.82	0.16	45.97	1.70
9	450.29	0.16	46.02	1.26
12	450.69	0.16	46.10	1.34
15	450.70	0.16	45.99	1.97
18	450.21	0.16	45.98	1.31
21	449.80	0.16	46.15	1.99
24	447.68	0.16	45.68	1.67
27	442.52	0.16	45.20	1.11
30	432.20	0.16	44.09	2.21
33	409.39	0.16	41.06	2.27
36	366.87	0.16	36.03	1.20
39	299.09	0.17	28.32	1.59
42	210.74	0.17	19.16	1.37
45	128.60	0.18	10.89	1.19
48	68.32	0.19	5.09	0.67
51	32.20	0.19	2.13	0.68
54	13.64	0.20	0.67	1.54
57	5.83	0.20	0.20	0.77
60	2.22	0.20	0.05	0.70
63	0.41	0.20	0.00	0.82
66	0.54	0.20	0.01	0.82

^{252}Cf and AmLi Background count rates from MCNP simulations

	Singles	Singles Error	Doubles	Doubles Error
^{252}Cf	431.64	0.10	3.48	1.10
AmLi	182.67	0.26	0.00	0.00
^{252}Cf in fuel through hole	1102.60	0.06	23.35	0.43

MCNP results of MTR Assembly L-108; with ^{252}Cf and AmLi

	Singles	Singles Error	Doubles	Doubles Error
Mid scan with ^{252}Cf	882.64	0.13	49.73	0.61
Mid scan-^{252}Cf/ rotated 90 deg	806.99	0.13	43.78	0.65
Bottom-^{252}Cf/18cm	852.48	0.13	46.08	0.63
Mid scan-AmLi	616.68	0.26	26.22	1.40
Mid scan- ^{252}Cf inside fuel hole	2517.4	0.08	270.22	0.29

MCNP results of MTR Assembly L-108; with ^{252}Cf and AmLi minus background

	Singles	Singles Error	Doubles	Doubles Error
Mid scan with ^{252}Cf	451.00	0.16	46.25	1.26
Mid scan-^{252}Cf/ rotated 90 deg	375.35	0.16	40.31	1.28
Bottom-^{252}Cf/18cm	420.84	0.16	42.60	1.27
Mid scan-AmLi	434.01	0.37	26.22	1.40
Mid scan- ^{252}Cf inside fuel hole	1414.8	0.10	246.87	0.52

MCNP simulation results of the partial assembly; three-point scan with ^{252}Cf source

4-Plates Partial Assembly Scan with ^{252}Cf source				
	singles	singles error	Doubles	Doubles error
top point	527.05	0.16	10.77	1.17
middle point	530.01	0.16	10.90	1.16
bottom point	523.34	0.16	10.55	1.18
6-Plates Partial Assembly Scan with ^{252}Cf source				
Top scan	560.48	0.16	14.77	1.03
Middle Scan	564.08	0.15	15.02	1.01
Bottom Scan	554.10	0.15	14.38	1.03

8-Plates Partial Assembly Scan with ^{252}Cf source				
top point	640.42	0.14	20.32	0.89
middle point	646.30	0.14	20.74	0.89
bottom point	631.79	0.15	19.67	0.91
10-Plates Partial Assembly Scan with ^{252}Cf source				
top point	698.49	0.14	25.71	0.80
middle point	707.34	0.14	26.53	0.79
bottom point	689.06	0.14	25.24	0.81
12-Plates Partial Assembly Scan with ^{252}Cf source				
top point	754.61	0.14	31.62	0.73
middle point	764.04	0.13	32.74	0.73
bottom point	741.60	0.14	30.65	0.75
14-Plates Partial Assembly Scan with ^{252}Cf source				
top point	807.58	0.13	38.17	0.68
middle point	820.10	0.13	39.67	0.67
bottom point	792.77	0.13	36.78	0.70
16-Plates Partial Assembly Scan with ^{252}Cf source				
top point	849.06	0.13	43.45	0.64
middle point	862.73	0.13	45.09	0.63
bottom point	832.24	0.13	41.75	0.66
18-Plates Partial Assembly Scan with ^{252}Cf source				
top point	882.50	0.13	47.95	0.62
middle point	896.27	0.13	49.31	0.61
bottom point	863.47	0.13	45.20	0.63
19-Plates Partial Assembly Scan with ^{252}Cf source				

top point	870.73	0.13	48.04	0.62
middle point	882.64	0.13	49.73	0.61
bottom point	852.48	0.13	46.08	0.63

MCNP simulation results of the partial assembly; with ^{252}Cf source minus background

4-Plates Partial Assembly Scan with ^{252}Cf source				
	singles	singles error	Doubles	Doubles error
top point	95.41	0.19	7.30	1.61
middle point	98.37	0.19	7.43	1.60
bottom point	91.70	0.19	7.07	1.61
6-Plates Partial Assembly Scan with ^{252}Cf source				
Top scan	128.84	0.19	11.29	1.51
Middle Scan	132.44	0.18	11.54	1.49
Bottom Scan	122.46	0.18	10.90	1.51
8-Plates Partial Assembly Scan with ^{252}Cf source				
top point	208.78	0.17	16.84	1.41
middle point	214.66	0.17	17.26	1.41
bottom point	200.15	0.18	16.20	1.43
10-Plates Partial Assembly Scan with ^{252}Cf source				
top point	266.85	0.17	22.23	1.36
middle point	275.70	0.17	23.05	1.35
bottom point	257.42	0.17	21.77	1.37
12-Plates Partial Assembly Scan with ^{252}Cf source				
top point	322.97	0.17	28.14	1.32
middle point	332.40	0.16	29.26	1.32
bottom point	309.96	0.17	27.17	1.33

14-Plates Partial Assembly Scan with ^{252}Cf source				
top point	375.94	0.16	34.70	1.29
middle point	388.46	0.16	36.19	1.29
bottom point	361.13	0.16	33.30	1.30
16-Plates Partial Assembly Scan with ^{252}Cf source				
top point	417.42	0.16	39.97	1.27
middle point	431.09	0.16	41.61	1.27
bottom point	400.60	0.16	38.28	1.28
18-Plates Partial Assembly Scan with ^{252}Cf source				
top point	450.86	0.16	44.47	1.26
middle point	464.63	0.16	45.84	1.26
bottom point	431.83	0.16	41.73	1.27
19-Plates Partial Assembly Scan with ^{252}Cf source				
top point	439.09	0.16	44.57	1.26
middle point	451.00	0.16	46.25	1.26
bottom point	420.84	0.16	42.60	1.27

MCNP simulation results of the partial assembly; three-point scan with AmLi source

4-Plates Partial Assembly Scan with AmLi source				
	singles	singles error	Doubles	Doubles error
top point	282.01	0.37	4.02	3.24
middle point	283.87	0.37	4.08	3.25
bottom point	260.81	0.39	3.73	3.42
6-Plates Partial Assembly Scan with AmLi source				
Top scan	317.83	0.36	6.15	2.67
Middle Scan	319.73	0.35	6.20	2.67

Bottom Scan	313.73	0.36	5.97	2.73
8-Plates Partial Assembly Scan with AmLi source				
top point	390.26	0.32	9.19	2.22
middle point	394.46	0.32	9.44	2.22
bottom point	384.72	0.32	8.89	2.27
10-Plates Partial Assembly Scan with AmLi source				
top point	448.47	0.30	12.88	1.91
middle point	454.10	0.30	13.35	1.87
bottom point	440.30	0.31	12.56	1.93
12-Plates Partial Assembly Scan with AmLi source				
top point	504.59	0.29	16.64	1.71
middle point	511.80	0.29	17.37	1.69
bottom point	493.38	0.29	16.08	1.75
14-Plates Partial Assembly Scan with AmLi source				
top point	551.30	0.28	19.68	1.56
middle point	560.68	0.27	20.55	1.54
bottom point	541.18	0.28	19.23	1.59
16-Plates Partial Assembly Scan with AmLi source				
top point	598.09	0.27	23.40	1.48
middle point	608.09	0.26	24.43	1.46
bottom point	585.39	0.27	22.90	1.51
18-Plates Partial Assembly Scan with AmLi source				
top point	627.440	0.26	25.279	1.41
middle point	638.010	0.26	26.550	1.4
bottom point	612.260	0.26	24.410	1.45
19-Plates Partial Assembly Scan with AmLi source				

top point	607.70	0.27	25.26	1.43
middle point	616.68	0.26	26.22	1.40
bottom point	593.53	0.27	24.71	1.45

MCNP simulation results of the partial assembly; with AmLi source minus background

4-Plates Partial Assembly Scan with AmLi source				
	singles	singles error	Doubles	Doubles error
top point	119.61	0.38	4.84	3.42
middle point	121.84	0.38	4.92	3.43
bottom point	94.08	0.40	4.49	3.59
6-Plates Partial Assembly Scan with AmLi source				
Top scan	162.73	0.44	7.41	2.08
Middle Scan	165.02	0.44	7.46	2.05
Bottom Scan	157.80	0.44	7.19	2.11
8-Plates Partial Assembly Scan with AmLi source				
top point	249.94	0.34	11.06	2.48
middle point	255.00	0.34	11.36	2.48
bottom point	243.27	0.34	10.71	2.52
10-Plates Partial Assembly Scan with AmLi source				
top point	320.02	0.32	15.51	2.20
middle point	326.80	0.32	16.07	2.17
bottom point	310.19	0.33	15.12	2.22
12-Plates Partial Assembly Scan with AmLi source				
top point	387.59	0.31	20.04	2.03
middle point	396.27	0.31	20.91	2.02
bottom point	374.09	0.31	19.36	2.07

14-Plates Partial Assembly Scan with AmLi source				
top point	443.83	0.30	23.70	1.91
middle point	455.12	0.29	24.74	1.89
bottom point	431.65	0.30	23.15	1.93
16-Plates Partial Assembly Scan with AmLi source				
top point	500.17	0.29	28.17	1.84
middle point	512.21	0.28	29.42	1.83
bottom point	484.87	0.29	27.57	1.87
18-Plates Partial Assembly Scan with AmLi source				
top point	535.50	0.28	30.44	1.79
middle point	548.23	0.28	31.97	1.78
bottom point	517.23	0.28	29.39	1.82
19-Plates Partial Assembly Scan with AmLi source				
top point	511.74	0.29	30.42	1.80
middle point	522.55	0.28	31.57	1.78
bottom point	494.68	0.29	29.75	1.82

Comparison of top, middle, and bottom count rates with the average in case of ^{252}Cf

^{235}U Mass	Top		Middle		Bottom		Average	
	S	D	S	D	S	D	S	D
48.78	95.41	7.30	98.37	7.43	91.70	7.07	95.16	7.26
73.16	128.84	11.29	132.44	11.54	122.46	10.90	127.91	11.25
97.55	208.78	16.84	214.66	17.26	200.15	16.20	207.86	16.77
121.94	266.85	22.23	275.70	23.05	257.42	21.77	266.66	22.35
146.33	322.97	28.14	332.40	29.26	309.96	27.17	321.78	28.19
170.72	375.94	34.70	388.46	36.19	361.13	33.30	375.18	34.73

195.10	417.42	39.97	431.09	41.61	400.60	38.28	416.37	39.95
219.49	450.86	44.47	464.63	45.84	431.83	41.73	449.11	44.01
231.69	439.09	44.57	451.00	46.25	420.84	42.60	436.98	44.47

Comparison of top, middle, and bottom count rates with the average in case of AmLi

^{235}U Mass	Top		Middle		Bottom		Average	
	S	D	S	D	S	D	S	D
48.78	119.61	4.84	121.84	4.92	94.08	4.49	111.84	4.75
73.16	162.73	7.41	165.02	7.46	157.80	7.19	161.85	7.35
97.55	249.94	11.06	255.00	11.36	243.27	10.71	249.40	11.04
121.94	320.02	15.51	326.80	16.07	310.19	15.12	319.00	15.57
146.33	387.59	20.04	396.27	20.91	374.09	19.36	385.99	20.11
170.72	443.83	23.70	455.12	24.74	431.65	23.15	443.53	23.86
195.10	500.17	28.17	512.21	29.42	484.87	27.57	499.08	28.39
219.49	535.50	30.44	548.23	31.97	517.23	29.39	533.65	30.60
231.69	511.74	30.42	522.55	31.57	494.68	29.75	509.65	30.58

APPENDIX C.

MCNP 6.1.1 MODEL

MID-POINT SCAN WITH ^{252}CF

Advanced Experimental Fuel Counter (AEFC)
c
c Fresh MTR measurements at LANL
c Cf interrogating source, full MTR assembly
c
c AMLI Original CASE
c Modified:
c * March 2014 by Karen Miller - Cf neutron benchmark, new lead version
c * July 2015 by Karen Miller - Addition of IRT-4M & ion chamber
c * February 2016 by Alexis Trahan - Restructure of input deck, surfaces and cells
c * November 2016 by J. Joshi and B. Adigun
c
c ---
c   CELL CARDS
c ---
c
100   1   -7.9   -101 102 -103 104   imp:n=1 $ SS shell main body
101   1   -7.9   -106 103 -108 110 400   imp:n=1 $ SS lid of main body
102   1   -7.9   -101 -104 105 111   imp:n=1 $ SS main body bottom
103   1   -7.9   -110 111 104 -108   imp:n=1 $ SS tube for fuel pass-thru
104   1   -7.9   -112 110 -103 113 400   imp:n=1 $ SS flange for fuel pass-
thru tube
105   1   -7.9   -106 101 -103 107   imp:n=1 $ SS flange for main body
c
110   3   -11.34   -120 110 -121 104 #(-122 110 -123)
          #(-120 110 -124 123)   imp:n=1 $ Pb shield
111   1   -7.9   -122 120 -121 104 110 #(-122 120 -123)   imp:n=1 $ outer SS tube for
lead shield
112   15 -9.58E-04 -122 110 -123   imp:n=1 $ hole in lead shield
113   1   -7.9   -120 110 -124 123   imp:n=1 $ SS outer layer of hole in
lead shield
115   1   -7.9   115 -116   imp:n=1 $ Funnel
c
c *** Detectors ***
c   mat den   surfaces   importance
201   3   -11.34   -231 221 -250 251   imp:n=1 $ Pb shield for tube #1
202   3   -11.34   -232 222 -250 251 231   imp:n=1 $ Pb shield for tube #2
203   3   -11.34   -233 223 -250 251   imp:n=1 $ Pb shield for tube #3
204   3   -11.34   -234 224 -250 251 233   imp:n=1 $ Pb shield for tube #4
205   3   -11.34   -235 225 -250 251   imp:n=1 $ Pb shield for tube #5
206   3   -11.34   -236 226 -250 251 235   imp:n=1 $ Pb shield for tube #6
c
211   4   -2.7   -221 201 -252 251   imp:n=1 $ Al body for tube #1
212   4   -2.7   -222 202 -252 251   imp:n=1 $ Al body for tube #2
213   4   -2.7   -223 203 -252 251   imp:n=1 $ Al body for tube #3

```
214   4   -2.7    -224 204 -252 251              imp:n=1 $ Al body for tube #4
215   4   -2.7    -225 205 -252 251              imp:n=1 $ Al body for tube #5
216   4   -2.7    -226 206 -252 251              imp:n=1 $ Al body for tube #6
c
c 221  5   -2.3    -211 201 -252 251              imp:n=1 $ Boron liner for tube #1
c 222  5   -2.3    -212 202 -252 251              imp:n=1 $ Boron liner for tube #2
c 223  5   -2.3    -213 203 -252 251              imp:n=1 $ Boron liner for tube #3
c 224  5   -2.3    -214 204 -252 251              imp:n=1 $ Boron liner for tube #4
c 225  5   -2.3    -215 205 -252 251              imp:n=1 $ Boron liner tube #5
c 226  5   -2.3    -216 206 -252 251              imp:n=1 $ Boron liner tube #6
c
231   6 -4.991e-4  -201 -253 254                  imp:n=1 $ active 4atm region of 3He
tube #1
232   6 -4.991e-4  -202 -253 254                  imp:n=1 $ active 4atm region of 3He
tube #2
233   6 -4.991e-4  -203 -253 254                  imp:n=1 $ active 4atm region of 3He
tube #3
234   6 -4.991e-4  -204 -253 254                  imp:n=1 $ active 4atm region of 3He
tube #4
235   6 -4.991e-4  -205 -253 254                  imp:n=1 $ 4 atm of 3He tube #5
236   6 -4.991e-4  -206 -253 254                  imp:n=1 $ 4 atm of 3He tube #6
c
241   6 -4.991e-4  -201 -252 253                  imp:n=1 $ top dead region of tube #1
242   6 -4.991e-4  -202 -252 253                  imp:n=1 $ top dead region of tube #2
243   6 -4.991e-4  -203 -252 253                  imp:n=1 $ top dead region of tube #3
244   6 -4.991e-4  -204 -252 253                  imp:n=1 $ top dead region of tube #4
245   6 -4.991e-4  -205 -252 253                  imp:n=1 $ top dead region of tube #5
246   6 -4.991e-4  -206 -252 253                  imp:n=1 $ top dead region of tube #6
c
251   6 -4.991e-4  -201 -254 251                  imp:n=1 $ bottom dead region of
tube #1
252   6 -4.991e-4  -202 -254 251                  imp:n=1 $ bottom dead region of
tube #2
253   6 -4.991e-4  -203 -254 251                  imp:n=1 $ bottom dead region of
tube #3
254   6 -4.991e-4  -204 -254 251                  imp:n=1 $ bottom dead region of
tube #4
255   6 -4.991e-4  -205 -254 251                  imp:n=1 $ bottom dead region of
tube #5
256   6 -4.991e-4  -206 -254 251                  imp:n=1 $ bottom dead region of
tube #6
c
261   4   -1.83   -221 -255 252                  imp:n=1 $ preamp for tube #1
262   4   -1.83   -222 -255 252                  imp:n=1 $ preamp for tube #2
263   4   -1.83   -223 -255 252                  imp:n=1 $ preamp for tube #3
264   4   -1.83   -224 -255 252                  imp:n=1 $ preamp for tube #4
```

```
265   4   -1.83    -225 -255 252                    imp:n=1  $ preamp for tube #5
266   4   -1.83    -226 -255 252                    imp:n=1  $ preamp for tube #6
c
271   2   -0.96    -241 #261                    imp:n=1  $ poly sleeve on top of tube #1
272   2   -0.96    -242 #262 #271                 imp:n=1  $ poly sleeve on top of tube
#2
273   2   -0.96    -243 #263                    imp:n=1  $ poly sleeve on top of tube #3
274   2   -0.96    -244 #264 #273                 imp:n=1  $ poly sleeve on top of tube
#4
275   2   -0.96    -245 #265                    imp:n=1  $ poly sleeve on top of tube #5
276   2   -0.96    -246 #266 #275                 imp:n=1  $ poly sleeve on top of tube
#6
c
300   2   -0.96    -102 104 -260 #(-122 -260 104)              $ Outside SS for lead
shield
             #(-231 -260 104) #(-232 -260 104)              $ 4 lead tubes (dets 1-4)
             #(-233 -260 104) #(-234 -260 104)
             #(-300 301 -302 -102 -260 104)              $ 4 air gaps
             #(-303 304 -302 -102 -260 104)
             #(-301 303 -302 305 -260 104)  110           $ Outside fuel pass thru tube
             #(104 -260  303 -301 -102 -305) #306           $ Outside new poly filler
             #(-400 -260 401) #310            imp:n=1  $ Guide tube for source, main
poly insert
301  15 -9.58E-04 -150 260 -103  #(-110 104 -103)           $ Outside pass thru tube
             #(-112 110 -103 113)              $ Outside pass thru tube flange
             #(-122 -121 260 110) #(-400 -103 260)           $ Outside lead shield,
interrogation tube
             #261 #262 #263 #264 #265 #266              $ Outside detectors
             #201 #202 #203 #204 #205 #206
             #271 #272 #273 #274 #275 #276 602        imp:n=1 $ air space above poly
302   2   -0.96    -102  150  260 -103            imp:n=1  $ poly sleeve
303  15 -9.58E-04  -300  301 -302 -102 -260 104        imp:n=1 $ air gap
304  15 -9.58E-04  -303  304 -302 -102 -260 104        imp:n=1 $ air gap
305  15 -9.58E-04  -301  303 -302  305 -260 104        imp:n=1 $ air gap
306   2   -0.96    104 -260 252 -153 -204 155 122 110    imp:n=1 $ new poly filler
307   2   -0.96    104 -260 303 -301 -102 -305 #(-236 -260 104)
             #(-235 -260  104) #309            imp:n=1  $ new poly in auxiliary
moderator
308  15 -9.58E-04 -151  104 -105  122 110              imp:n=1 $ new air gap
309   3  -11.34     303 -301  270 -305 104 -271        imp:n=1 $ Pb shield under
auxiliary moderator
310   3  -11.34     272 -273 -274  302 104 -271 151
             275 276                    imp:n=1  $ Pb shield under main moderator
c
c  *** Interrogation Source Vessel ***
c
```

```
c    mat   den    surfaces                  importance
400   0         403 -405 -404 402              imp:n=1 $ source cavity, outside Cf
source
401   2   -0.96   414 -412 -411 #(403 -405 -404)      imp:n=1 $ source vessel, poly
402   9   -0.01   -402                   imp:n=1 $ point source cell
403   0         -415 -413  414 #(414 -412 -411)     imp:n=1 $ void tube for AmLi
guide
404   1   -7.9   -400 -413  401 #(-415 -413 414)     imp:n=1 $ SS guide tube for
interrogation source
c
c *** Ionization Chamber ***
c
c    mat   den    surfaces                  importance
600   14  -2.133E-2  -600                 imp:n=1 $ IC gas fill
601   1   -7.9      -601 600              imp:n=1 $ IC wall
602   11  -19.25     -602 601              imp:n=1 $ tungsten shield
c
c L-108 Fuel Assembly
c
700 12 -1.0 -997              u=4 imp:n=1  $ PoolWater
705 10 -3.308 703 -707 705 -706 708 -704 u=12 imp:n=1  $ Fuel Meat
706 4 -2.7 #705              u=12 imp:n=1  $ Fuel Clad
c
710 0 715 -718 716 -717 -711 719 -720 u=14 FILL=12 (601) imp:n=1  $
TestAssemSlot0a
711 0 715 -718 716 -717 -711 721 -722 u=14 FILL=12 (602) imp:n=1  $
TestAssemSlot00a
712 0 715 -718 716 -717 -711 723 -724 u=14 FILL=12 (603) imp:n=1  $
TestAssemSlot01a
c 713 0 715 -718 716 -717 -711 725 -726 u=14 FILL=12 (604) imp:n=1  $
TestAssemSlot02a
c 714 0 715 -718 716 -717 -711 727 -728 u=14 FILL=12 (605) imp:n=1  $
TestAssemSlot03a
c 715 0 715 -718 716 -717 -711 729 -730 u=14 FILL=12 (606) imp:n=1  $
TestAssemSlot04a
c 716 0 715 -718 716 -717 -711 731 -732 u=14 FILL=12 (607) imp:n=1  $
TestAssemSlot05a
c 717 0 715 -718 716 -717 -711 733 -734 u=14 FILL=12 (608) imp:n=1  $
TestAssemSlot06a
c 718 0 715 -718 716 -717 -711 735 -736 u=14 FILL=12 (609) imp:n=1  $
TestAssemSlot07a
c 719 0 715 -718 716 -717 -711 737 -738 u=14 FILL=12 (610) imp:n=1  $
TestAssemSlot08a
c 720 0 715 -718 716 -717 -711 739 -740 u=14 FILL=12 (611) imp:n=1  $
TestAssemSlot09a
```

```
c 721 0 715 -718 716 -717 -711 741 -742 u=14 FILL=12 (612) imp:n=1   $
TestAssemSlot10a
c 722 0 715 -718 716 -717 -711 743 -744 u=14 FILL=12 (613) imp:n=1   $
TestAssemSlot11a
c 723 0 715 -718 716 -717 -711 745 -746 u=14 FILL=12 (614) imp:n=1   $
TestAssemSlot12a
c 724 0 715 -718 716 -717 -711 747 -748 u=14 FILL=12 (615) imp:n=1   $
TestAssemSlot13a
c 725 0 715 -718 716 -717 -711 749 -750 u=14 FILL=12 (616) imp:n=1   $
TestAssemSlot14a
726 0 715 -718 716 -717 -711 751 -752 u=14 FILL=12 (617) imp:n=1   $
TestAssemSlot15a
727 0 715 -718 716 -717 -711 757 -758 u=14 FILL=12 (618) imp:n=1   $
TestAssemSlot18a
728 0 715 -718 716 -717 -711 759 -760 u=14 FILL=12 (619) imp:n=1   $
TestAssemSlot19a
c
730 0 716 -717  718             u=14 FILL=4 imp:n=1   $ TestAssemAqua1a
731 0 716 -717 -715             u=14 FILL=4 imp:n=1   $ TestAssemAqua2a
732 0 715 -718  716 -717 (711 : -759) u=14 FILL=4 imp:n=1   $ TestAssemAqua3a
c
739 0 715 -718 716 -717 -711 720     u=14 FILL=4 imp:n=1   $ TestAssemGap0a
740 0 715 -718 716 -717 -711 722 -719 u=14 FILL=4 imp:n=1   $ TestAssemGap00a
741 0 715 -718 716 -717 -711 724 -721 u=14 FILL=4 imp:n=1   $ TestAssemGap01a
c 742 0 715 -718 716 -717 -711 726 -723 u=14 FILL=4 imp:n=1   $ TestAssemGap02a
c 743 0 715 -718 716 -717 -711 728 -725 u=14 FILL=4 imp:n=1   $ TestAssemGap03a
c 744 0 715 -718 716 -717 -711 730 -727 u=14 FILL=4 imp:n=1   $ TestAssemGap04a
c 745 0 715 -718 716 -717 -711 732 -729 u=14 FILL=4 imp:n=1   $ TestAssemGap05a
c 746 0 715 -718 716 -717 -711 734 -731 u=14 FILL=4 imp:n=1   $ TestAssemGap06a
c 747 0 715 -718 716 -717 -711 736 -733 u=14 FILL=4 imp:n=1   $ TestAssemGap07a
c 748 0 715 -718 716 -717 -711 738 -735 u=14 FILL=4 imp:n=1   $ TestAssemGap08a
c 749 0 715 -718 716 -717 -711 740 -737 u=14 FILL=4 imp:n=1   $ TestAssemGap09a
c 750 0 715 -718 716 -717 -711 742 -739 u=14 FILL=4 imp:n=1   $ TestAssemGap10a
c 751 0 715 -718 716 -717 -711 744 -741 u=14 FILL=4 imp:n=1   $ TestAssemGap11a
c 752 0 715 -718 716 -717 -711 746 -743 u=14 FILL=4 imp:n=1   $ TestAssemGap12a
c 753 0 715 -718 716 -717 -711 748 -745 u=14 FILL=4 imp:n=1   $ TestAssemGap13a
c 754 0 715 -718 716 -717 -711 750 -747 u=14 FILL=4 imp:n=1   $ TestAssemGap14a
755 0 715 -718 716 -717 -711 752 -723 u=14 FILL=4 imp:n=1   $ TestAssemGap15a
756 0 715 -718 716 -717 -711 758 -751 u=14 FILL=4 imp:n=1   $ TestAssemGap18a
757 0 715 -718 716 -717 -711 760 -757 u=14 FILL=4 imp:n=1   $ TestAssemGap19a
c
760 2 -2.7 710 -712 713 -716 -720 -711 u=14       imp:n=1   $ TestAssemPanel1a
761 0 -716 #760             u=14 FILL=4 imp:n=1   $ TestAssemPanel1Gapa
762 2 -2.7 710 -712 717 -714 -720 -711 u=14       imp:n=1   $ TestAssemPanel2a
763 0 717 #762             u=14 FILL=4 imp:n=1   $ TestAssemPanel2Gapa
c
```

770 0 780 -781 -782 -783 784 -785   FILL=14 (620)   imp:n=1 $ Final L-108 fuel
assembly
c
c *** Universe ***
c
c   mat   den   surfaces   importance
996   12 -1.0   -998 111 #(-101 -108 105) #(-106 101 -103 107)
             #(-106 101 103 -108) #(-400 108 -413)   imp:n=1 $ water
997   12 -1.0   -998 -111 #770 #115   imp:n=1 $ water
998   2   -2.35   998 -999   imp:n=1 $ pvc tank
999   0   999   imp:n=0 $ the nothing

c --
c   SURFACE CARDS
c --
c
c *** Detector Body ***
c
101   cz   17.098 $ outer radius of main body
102   cz   16.78 $ inner radius of main body
103   pz   46.72 $ top of main body
104   pz   0.0 $ bottom of main body
105   pz   -0.3175 $ bottom of main body
106   cz   18.529 $ main body flange outer radius
107   pz   46.08 $ main body flange bottom
108   pz   47.5074 $ top of main body lid
c
110   c/z   0 4.29 6.17 $ outer radius of fuel pass-thru tube
111   c/z   0 4.29 5.85 $ inner radius of fuel pass-thru tube
112   c/z   0 4.29 7.42 $ fuel pass-thru flange outer radius
113   pz   45.45 $ fuel pass-thru flange bottom
c   Vx   Vy   Vz   Hx   Hy   Hz   R
115   rcc   0 4.29 46.73 0   0   10   5.74 $ inner radius of funnel
116   rcc   0 4.29 46.73 0   0   10   5.84 $ outer radius of funnel
c
120   c/z   0 2.54 7.239 $ outer radius of lead shield
121   pz   43.85 $ top of lead shield
122   c/z   0 2.54 7.477 $ outer radius of SS tube for lead shield
123   c/y   0 40.32 0.9525 $ hole in Pb shield
124   c/y   0 40.32 1.1049 $ SS layer for hole in lead shield
c
150   cz   16.61 $ poly liner
151   c/z   0 2.24 7.4777 $ inner radius of poly for air gap (mts)
152   px   -7.477
153   px   7.477
154   py   11.32

```
155  py     2.54
c
c DETECTORS
c          Vx   Vy    R
201  C/Z   -8.61  -3.22  1.188945     $ B inner radius for tube #1
202  C/Z   -5.98  -6.59  1.188945     $ B inner radius for tube #2
203  C/Z    8.61  -3.22  1.188945     $ B inner radius for tube #3
204  C/Z    5.98  -6.59  1.188945     $ B inner radius for tube #4
205  C/Z    2.19  -13.27 1.18882      $ B inner radius for tube #5
206  C/Z   -2.19  -13.27 1.18882      $ B inner radius for tube #6
c
211  C/Z   -8.61  -3.22  1.189        $ Al inner radius for tube #1
212  C/Z   -5.98  -6.59  1.189        $ Al inner radius for tube #2
213  C/Z    8.61  -3.22  1.189        $ Al inner radius for tube #3
214  C/Z    5.98  -6.59  1.189        $ Al inner radius for tube #4
215  C/Z    2.19  -13.27 1.189        $ Al inner radius for tube #5
216  C/Z   -2.19  -13.27 1.189        $ Al inner radius for tube #6
c
221  C/Z   -8.61  -3.22  1.27         $ Al outer radius for tube #1
222  C/Z   -5.98  -6.59  1.27         $ Al outer radius for tube #2
223  C/Z    8.61  -3.22  1.27         $ Al outer radius for tube #3
224  C/Z    5.98  -6.59  1.27         $ Al outer radius for tube #4
225  C/Z    2.19  -13.27 1.27         $ Al outer radius for tube #5
226  C/Z   -2.19  -13.27 1.27         $ Al outer radius for tube #6
c
231  C/Z   -8.61  -3.22  2.2225       $ Pb outer radius for tube #1
232  C/Z   -5.98  -6.59  2.2225       $ Pb outer radius for tube #2
233  C/Z    8.61  -3.22  2.2225       $ Pb outer radius for tube #3
234  C/Z    5.98  -6.59  2.2225       $ Pb outer radius for tube #4
235  C/Z    2.19  -13.27 2.2225       $ Pb outer radius for tube #5
236  C/Z   -2.19  -13.27 2.2225       $ Pb outer radius for tube #6
c          Vx   Vy    Vz   Hx  Hy  Hz  R
241  RCC  -8.61 -3.22   34.76 0.0 0.0 1.3 2.2225 $ poly sleeve on top of tube #1
242  RCC  -5.98 -6.59   34.76 0.0 0.0 1.3 2.2225 $ poly sleeve on top of tube #2
243  RCC   8.61 -3.22   34.76 0.0 0.0 1.3 2.2225 $ poly sleeve on top of tube #3
244  RCC   5.98 -6.59   34.76 0.0 0.0 1.3 2.2225 $ poly sleeve on top of tube #4
245  RCC   2.19 -13.27  34.76 0.0 0.0 1.3 2.2225 $ poly sleeve on top of tube #5
246  RCC  -2.19 -13.27  34.76 0.0 0.0 1.3 2.2225 $ poly sleeve on top of tube #6
c
250  PZ    34.76              $ Top of Pb tubes
251  PZ    1.280              $ Bottom of Pb tubes
252  PZ    32.40              $ Top of Al tube
253  PZ    29.54              $ Top of active region
254  PZ    4.140              $ Bottom of active region
255  PZ    41.29              $ Top of preamps
256  PZ    36.06              $ Top of tube poly sleeves
```

```
260  PZ     33.69                 $ Bottom of poly sleeve
270  py     -15.59                 $ side surface for Pb under auxiliary moderator
271  pz     1.28                  $ top surface for Pb under auxiliary moderator
272  px     -11.0                 $ Pb shield under 4 tubes
273  px     11.0                  $ Pb shield under 4 tubes
274  py     -0.75                 $ Pb shield under 4 tubes
275  p      1.0  1.0  0.0  -16.657   $ Pb shield under 4 tubes
276  p      -1.0  1.0  0.0  -16.657   $ Pb shield under 4 tubes
c
c
300  px     6.248                 $ air gap around auxiliary moderator
301  px     6.197                 $ air gap around auxiliary moderator
302  py     -10.46                $ air gap around auxiliary moderator
303  px     -6.197                $ air gap around auxiliary moderator
304  px     -6.248                $ air gap around auxiliary moderator
305  py     -10.51                $ air gap around auxiliary moderator
c
400  c/z    0.0  13.47  2.0        $ guide tube for interrogation source
401  pz     11.69                 $ bottom of guide tube for interrogation source
402  s      0  13.47  13.7725  1e-6    $ SPHERE OF CF in interrogation tube
403  pz     13.2725               $ source cavity bottom
404  c/z    0  13.47  1.334        $ source cavity outer
405  pz     17.56                 $ source cavity top
410  pz     12.480                $ source vessel bottom
411  c/z    0  13.47  1.5875        $ source vessel outer
412  pz     18.83                 $ source vessel top
413  pz     50.32                 $ top of void in source tube
414  pz     12.48                 $ bottom of void in source tube
415  c/z    0.0  13.47  1.7         $ guide tube for interrogation source inner radius
c *** Ionization Chamber ***
c
c      Vx  Vy   Vz   Hx  Hy  Hz  R
600 rcc  0 -5.1524 40.32  0 -3.8252 0  0.9776  $ inner IC wall
601 rcc  0 -5     40.32  0 -4.13  0  1.13    $ outer IC wall
602 rcc  0 -5     40.32  0 -4.13  0  2.145   $ outer tungsten shield wall
c
c *** MTR Fuel ***
703 PZ -8.25                     $ TestAssemFuelStrip_Bottom
704 P   3.12377 -13.72501 0.0 42.72073   $ TestAssemFuelStrip_East
705 C/Z 13.676 0.0 14.0625           $ TestAssemFuelStrip_Inner
706 C/Z 13.676 0.0 14.08950            $ TestAssemFuelStrip_Outer
707 PZ  51.75                    $ TestAssemFuelStrip_Top
708 P -3.12377 -13.72501 0.0 -42.72073   $ TestAssemFuelStrip_West
c
709 PX -4.048                    $ TestAssemPanel_Back
710 PZ -9.5                      $ TestAssemPanel_Bottom
```

```
711  PX 4.048                    $ TestAssemPanel_Front
712  PZ 54                       $ TestAssemPanel_Top
c
713  PY -3.9519                   $ TestAssemPanel1_Left
714  PY 3.9519                    $ TestAssemPanel2_Right
c
715  PZ -8.75                    $ TestAssemSlot_Bottom
716  PY -3.556                   $ TestAssemSlot_Left
717  PY 3.556                    $ TestAssemSlot_Right
718  PZ  52.25                   $ TestAssemSlot_Top
c
719  C/Z 9.779 0.0 13.9998   $ TestAssemSlot0_Inner
720  C/Z 9.779 0.0 14.1522   $ TestAssemSlot0_Outer
721  C/Z 10.212 0.0 13.9998  $ TestAssemSlot00_Inner
722  C/Z 10.212 0.0 14.1522  $ TestAssemSlot00_Outer
723  C/Z 10.645 0.0 13.9998  $ TestAssemSlot01_Inner
724  C/Z 10.645 0.0 14.1522  $ TestAssemSlot01_Outer
725  C/Z 11.078 0.0 13.9998  $ TestAssemSlot02_Inner
726  C/Z 11.078 0.0 14.1522  $ TestAssemSlot02_Outer
727  C/Z 11.511 0.0 13.9998  $ TestAssemSlot03_Inner
728  C/Z 11.511 0.0 14.1522  $ TestAssemSlot03_Outer
729  C/Z 11.944 0.0 13.9998  $ TestAssemSlot04_Inner
730  C/Z 11.944 0.0 14.1522  $ TestAssemSlot04_Outer
731  C/Z 12.377 0.0 13.9998  $ TestAssemSlot05_Inner
732  C/Z 12.377 0.0 14.1522  $ TestAssemSlot05_Outer
733  C/Z 12.81 0.0 13.9998   $ TestAssemSlot06_Inner
734  C/Z 12.81 0.0 14.1522   $ TestAssemSlot06_Outer
735  C/Z 13.243 0.0 13.9998  $ TestAssemSlot07_Inner
736  C/Z 13.243 0.0 14.1522  $ TestAssemSlot07_Outer
737  C/Z 13.676 0.0 13.9998  $ TestAssemSlot08_Inner
738  C/Z 13.676 0.0 14.1522  $ TestAssemSlot08_Outer
739  C/Z 14.109 0.0 13.9998  $ TestAssemSlot09_Inner
740  C/Z 14.109 0.0 14.1522  $ TestAssemSlot09_Outer
741  C/Z 14.542 0.0 13.9998  $ TestAssemSlot10_Inner
742  C/Z 14.542 0.0 14.1522  $ TestAssemSlot10_Outer
743  C/Z 14.975 0.0 13.9998  $ TestAssemSlot11_Inner
744  C/Z 14.975 0.0 14.1522  $ TestAssemSlot11_Outer
745  C/Z 15.408 0.0 13.9998  $ TestAssemSlot12_Inner
746  C/Z 15.408 0.0 14.1522  $ TestAssemSlot12_Outer
747  C/Z 15.841 0.0 13.9998  $ TestAssemSlot13_Inner
748  C/Z 15.841 0.0 14.1522  $ TestAssemSlot13_Outer
749  C/Z 16.274 0.0 13.9998  $ TestAssemSlot14_Inner
750  C/Z 16.274 0.0 14.1522  $ TestAssemSlot14_Outer
751  C/Z 16.707 0.0 13.9998  $ TestAssemSlot15_Inner
752  C/Z 16.707 0.0 14.1522  $ TestAssemSlot15_Outer
753  C/Z 17.14 0.0 13.9998   $ TestAssemSlot16_Inner
```

```
754  C/Z 17.14 0.0 14.1522   $ TestAssemSlot16_Outer
755  C/Z 17.573 0.0 13.9998   $ TestAssemSlot17_Inner
756  C/Z 17.573 0.0 14.1522   $ TestAssemSlot17_Outer
757  C/Z 17.14 0.0 13.9998   $ TestAssemSlot18_Inner
758  C/Z 17.14 0.0 14.1522   $ TestAssemSlot18_Outer
759  C/Z 17.573 0.0 13.9998   $ TestAssemSlot19_Inner
760  C/Z 17.573 0.0 14.1522   $ TestAssemSlot19_Outer
c
780 999 pz -32.38
781 999 pz  75.88
782 999 C/Z 9.779 4.29 14.2   $ TestAssemSlot0_Outer px  -4.049
783 999 px   4.049
784 999 py   0.3
785 999 py   8.3
c
c *** Room ***
997  so  100
c       Vx  Vy  Vz A1x A1y A1z A2x A2y A2z A3x A3y A3z
c 998  box  -100 -150 -50 200 0.0 0.0 0.0 300  0.0 0.0 0.0 500 $ room, inner
surface
c 999  box  -115 -165 -65 230 0.0 0.0 0.0 330  0.0 0.0 0.0 515 $ room, outer
surface
998 rcc 0 0 -51.1175  0 0 152.4  63.5
999 rcc 0 0 -52.3875  0 0 153.67  64.135


c
c -------------------------------------------------------------
c                 TRANSFORMATIONS
c -------------------------------------------------------------
C L108 Fuel into Throat
*TR601 -3.897 0.0  0.0
*TR602 -3.464 0.0  0.0
*TR603 -3.031 0.0  0.0
c *TR604 -2.598 0.0  0.0
c *TR605 -2.165 0.0  0.0
c *TR606 -1.732 0.0  0.0
c *TR607 -1.299 0.0  0.0
c *TR608 -0.866 0.0  0.0
c *TR609 -0.433 0.0  0.0
c *TR610  0.0   0.0  0.0
c *TR611  0.433 0.0  0.0
c *TR612  0.866 0.0  0.0
c *TR613  1.299 0.0  0.0
c *TR614  1.732 0.0  0.0
c *TR615  2.165 0.0  0.0
c *TR616  2.598 0.0  0.0
```

```
*TR617  3.031 0.0  0.0
*TR618  3.464 0.0  0.0
*TR619  3.897 0.0  0.0
*TR620  0.0   4.29  -4.91  -90 -180 -90  0 -90 90  90 90 0
*TR999  -4.29 4.29  -4.91  -90 -180 -90  0 -90 90  90 90 0
c --------------------------------------------------------------
c                  MATERIAL CARDS
c --------------------------------------------------------------
c
c *** Material 1: Stainless Steel 304 ***
c
m1    26057      0.6908
      28058      0.0892
      24052      0.1900
      25055      0.0200
      14028      0.0100
      nlib=.70c
c
c *** Material 2: High Density Polyethylene ***
c
m2    1001       0.6667
      6000       0.3333
      nlib=.70c
mt2   poly.10t              $ s(a,b) treatment for poly
c
c *** Material 3: High Purity Lead ***
c
m3    82206      0.241
      82207      0.221
      82208      0.524
      nlib=.70c
c
c *** Material 4: Aluminum ***
c
m4    13027      1.0
      nlib=.70c
c
c *** Material 5: Boron-10 ***
c
c m5    5010      1.0
c      nlib=.70c
c
c *** Material 6: Helium-3 ***
c
m6    2003       1.0
      nlib=.70c
```

```
c
c *** Material 7: Cadmium ***
c
c m7    48000       1.0
c       nlib=.70c
c
c
c *** Material 9: Californium-252 ***
c
c
m9     98252       1.0
       nlib=.70c
c
c *** Material-10, fresh fuel ***
c
m10    92235   -0.35715
       92238   -0.02464
       13027   -0.61821
       nlib=.70c
c
c *** Material 11: Tungsten ***
c
m11    74182      -0.3
       74184      -0.3
       74186      -0.3
       28060      -0.06
       29063      -0.04
       nlib=.70c
c
c *** Material 12: Water ***
c
m12     8016       0.33333
        1001       0.66667
        nlib=.70c
mt12 lwtr.10t              $ s(a,b) treatment for water
c *** Material 14: Xenon gas fill in IC ***
m14   54129       0.264
      54130       0.0407
      54131       0.212
      54132       0.269
      nlib=.70c
c
m15   6000   -0.000124      $ Air (9.58e-4 g/cc in Los Alamos)
      7014   -0.755268      $ (from PNNL)
      8016   -0.231781
      18040  -0.012827
```

```
    nlib=.70c
c
c -------------------------------------------------------------
c                    SOURCE CARDS
c -------------------------------------------------------------
c
mode n
nps 1e7
sdef par=SF pos= 0  13.47 13.7725 WGT= 4.567E4
c sdef par=SF pos= 0  13.97 13.7725 WGT=1
prdmp j 1e8 1 2 5e6
c
c -------------------------------------------------------------
c                    TALLY CARDS
c -------------------------------------------------------------
c
c *f8:p  600
c
fc18   Doubles in Tubes 1-4
f18:n (231 232 233 234)
ft18 CAP 2003 GATE 450 12800
c
fc28   Doubles in Tubes 5-6
f28:n (235 236)
ft28 CAP 2003 GATE 450 12800
c
fc38   Doubles in Tubes 1-6
f38:n (231 232 233 234 235 236)
ft38 CAP 2003 GATE 450 12800
c
fc48   Singles in Tubes 1-4
f48:n (231 232 233 234)
ft48 CAP 2003
c
fc58   Singles in Tubes 5-6
f58:n (235 236)
ft58 CAP 2003
c
fc68   Singles in Tubes 1-6
f68:n (231 232 233 234 235 236)
ft68 CAP 2003
```

REFERENCES

1. "Einstein's letter to Roosevelt." August 2, 1939. (n.d.). Retrieved June 10, 2013, from http://www.dannen.com/ae-fdr.html.

2. Kelly, C. C., "The Manhattan project: the birth of the atomic bomb in the words of its creators, eyewitnesses, and historians." New York: Black Dog & Leventhal Publishers: Distributed by Workman Pub, USA; 2007.

3. Sagan, Scott D., "Why Do States Build Nuclear Weapons?: Three Models in Search of a Bomb." International Security, vol. 21, no. 3, 1996, pp. 54–86., www.jstor.org/stable/2539273.

4. Farlow, Troy Jay., "Gold Standard or Case-by-Case: Which Method Is Best for the Nonproliferation Regime?" Harvard University Library. ProQuest Dissertations Publishing, Mar. 2014. Web. 16 Feb. 2017.

5. Menlove HO, et al., "Field Tests of the AEFC for Verification of Research Reactor Spent Fuel at the WWR-SM Reactor at the Institute of Nuclear Physics Uzbekistan." proc. INMM Annual Meeting; Orlando, Florida USA; 2012.

6. Root M., "Technical Basis for the Use of a Correlated Neutron Source in the Uranium Neutron Coincidence Collar." Los Alamos National Laboratory, Los Alamos, NM USA; Publication in Process 2016.

7. Crane, T.W., M.P. Baker., "Neutron Detectors." Passive Nondestructive Assay Manual-PANDA. N.p.: Los Alamos National Laboratory, 2007. pp. 379-406.

8. Knoll, Glenn F., "Slow Neutron Detection." Radiation Detection and Measurement. 3rd. ed. New York: Wiley, 1999. Print.

9. Trahan A C., "Utilization of the Differential Die-Away Self-Interrogation Technique for Characterization and Verification of Spent Nuclear Fuel." University of Michigan; Ann Arbor, Michigan USA; 2016.

10. Ensslin, N., "Principles of Neutron Coincidence Counting." Passive Nondestructive Assay Manual-PANDA. N.p.: Los Alamos National Laboratory, 2007, pages 457-491.

11. Menlove HO., et al, "The development of a new, neutron, time correlated, interrogation method for measurement of ^{235}U content in LWR fuel assemblies." Nuclear Instruments and Methods in Physics; Volume 701, 2013.

12. Jehouani, J.C. Nimal, P. Reuss., "Comparison of mutual shielding and self-shielding powers of ^{235}U, ^{238}U, ^{239}Pu and ^{240}Pu." Annals of Nuclear Energy, Volume 19, Issue 4, 1992, Pages 195-202, ISSN 0306-4549.

13. Li Ke., "Study of SF of ^{252}Cf: Structure of Neutron-Rich Nuclei, Gamma-Ray Angular Correlation and G-factor Measurements." Vanderbilt University; Nashville, Tennessee USA; 2008.

14. Beckurt, K.H. & Wirtz, K.,"Neutron Physics-Neutron Sources." Springer-Verlag, Berlin 1964.

15. Reilly, N., Ensslin N., Smith Jr. H., Krehner S., "Passive Nondestructive Assay of Nuclear materials." Los Alamos National Laboratory, 1991, Page 342.

16. Lamarsh, John R., and Anthony John Baratta., "Introduction to Nuclear Engineering." Upper Saddle River, NJ: Prentice Hall, 2009. Print.

17. Menlove HO, et al., "The Optimization and Calibration of the AWCC Using 252Cf Interrogation and the Comparison with an AmLi Neutron Source." Los Alamos National Laboratory, USA, LA-UR-15-29620.

18. Trellue, HR., Tobin, SJ., "The State of Art of the Nondestructive Assay of Spent Fuel Assemblies." LA-UR- 16-20376, Los Alamos National Laboratory, USA, 02-25-2016.

19. Menlove, HO, et al., "The Advanced Experimental Fuel Counter – a Portable Detector for the Verification of Research Reactor Spent Fuel." LA-UR- 11-01586, Los Alamos National Laboratory, USA, 04-05-2011.

20. Menolve, Howard O, et al., "AEFC for the Verification of Research Reactor Spent Fuel – Field Experience to Date." Los Alamos National Laboratory, 16 Feb. 2017. Web. 14 Apr. 2017. <http://permalink.lanl.gov/object/tr?what=info:lanl-repo/lareport/LA-UR-17-21223>.

21. Glaser, Alexander. "The Conversion of Research Reactors to Low-Enriched Fuel and the Case of the FRM-II." Taylor and Francis, 31 May 2001. Web. 17 Apr. 2017. <http://scienceandglobalsecurity.org/archive/sgs10glaser.pdf>.

22. Ensslin, N, et al., "Application Guide to Neutron Multiplicity Counting." LA-13422-M, Los Alamos National Laboratory, 1998, pages 43-44.

VITA

Jay P Joshi was born and raised in Nepal, where he completed his education up to the High School. After he moved to the US he joined Austin Community College to acquire some college credits before he joined a BS Radiation Physics program at the University of Texas at Austin. He graduated with a BS in Radiation Physics from the University of Texas at Austin in December 2013. He started his MS degree in Nuclear Engineering in January 2015. He worked at the Los Alamos National Laboratory between May 2016 to May 2017, where he performed his MS research. He received his MS degree in Nuclear Engineering from the Missouri University of Science and Technology in July 2017.